UNLV | University Libraries
University of Nevada, Las Vegas

Effects of high-impedance-contrast boundary upon multi-modal seismic surface wave data

Prajwol Tamrakar
University of Nevada, Las Vegas

Follow this and additional works at: https://digitalscholarship.unlv.edu/thesesdissertations

Part of the Civil Engineering Commons, Geology Commons, Geophysics and Seismology Commons, and the Geotechnical Engineering Commons

EFFECTS OF HIGH-IMPEDANCE-CONTRAST BOUNDARY

UPON MULTI-MODAL SEISMIC SURFACE WAVE DATA

by

Prajwol Tamrakar

A thesis submitted in partial fulfillment
of the requirements for the

Master of Science in Engineering

Department of Civil and Environmental Engineering
Howard R. Hughes College of Engineering
The Graduate College

University of Nevada, Las Vegas
December 2011

THE GRADUATE COLLEGE

We recommend the thesis prepared under our supervision by

Prajwol Tamrakar

entitled

Effects of High-Impedance-Contrast Boundary Upon Multi-Modal Seismic Surface Wave Data

be accepted in partial fulfillment of the requirements for the degree of

Master of Science in Engineering
Department of Civil and Environmental Engineering

Barbara Luke, Committee Chair

Carlos Calderon-Macias, Committee Member

Douglas Rigby, Committee Member

Wanda Taylor, Graduate College Representative

Ronald Smith, Ph. D., Vice President for Research and Graduate Studies and Dean of the Graduate College

December 2011

ABSTRACT

Effects of high-impedance-contrast boundary

upon multi-modal seismic surface wave data

by

Prajwol Tamrakar

Dr. Barbara Luke, Examination Committee Chair
Professor, Civil and Environmental Engineering
Director, Applied Geophysics Center
University of Nevada, Las Vegas

Synthetic studies and analyses of an experimental dataset were conducted to address the use of Rayleigh-type surface waves for estimation of shear wave velocity (VS) profiles of shallow bedrock sites. The shallow bedrock presents a high impedance contrast boundary which causes surface wave energy to be partitioned to higher modes. Idealized studies of hypothetical datasets and root-mean-squared calculations of error surfaces showed that if reliable dispersion data are available over a broad frequency spectrum, the VS profile can be recovered using the fundamental mode alone. However, when dispersion data are limited to a relatively narrow frequency band representing what might be commonly sampled in practice, the fundamental mode alone is insufficient to resolve the VS profile, but joint consideration of higher modes along with the fundamental mode will be successful in some cases. Outcomes of similar tests on experimental data from a shallow bedrock site were instructive but less definitive. Tests repeatedly demonstrated that a good quality starting model is necessary to converge upon a reasonable solution. To improve the starting model, the dispersion dataset can be scrutinized to estimate depth to bedrock. Dispersion curves for the shallow bedrock case

are particularly susceptible to misinterpretation. Tests revealed that the consequences of a likely form of misinterpretation are strong velocity fluctuations and overestimation of VS of the bedrock.

ACKNOWLEDGEMENTS

Norma Biggar for her contribution on organizing chapter 1 of the thesis.

I would like to thank my colleagues of Applied Geophysics Center- Suchan Lamichhane, Pinthep Kittipongdaja, Nihad Rajabdeen and Helena Murvosh for their support during my research, and my friends, Eleeja Shrestha and Nipesh Pradhananga, for reviewing my thesis. I appreciate my father Laxmi Narayan Tamrakar, mother Sharmistha Tamrakar, sister Pratistha Tamrakar and brother Prafulla Tamrakar for their love, care, support and encouragement for pursuing my master degree in the United States.

In addition, I would like to acknowledge the Department of Civil and Environmental Engineering for providing a Teaching Assistantship in the first year of my master's degree and the UNLV Strategic Plan Graduate Research Assistants program for funding in the second year.

TABLE OF CONTENTS

LIST OF TABLES

LIST OF FIGURES

xiii

xiv

CHAPTER 1

INTRODUCTION AND BACKGROUND

1.1 Engineering need for site characterization

Mechanical properties of a layered subsurface such as density, Poisson's ratio and shear-wave velocity (VS) are required to understand certain site characteristics. For example, density and VS define shear stiffness of the layers. This information is essential for: a) determining one-dimensional (1-D) profiles or two-dimensional (2-D) slices of VS or shear stiffness showing variation with position, b) locating weak zones and voids in the subsurface, c) assessing potential for soil liquefaction, d) determining elastic moduli for settlement analysis, e) mapping the soil-bedrock interface, and more (Stokoe et al., 2004).

Shallowly buried, intact bedrock can be a favorable condition for the construction of stable foundations for superstructures and roadways. However, the bedrock at shallow depths can cause problems in excavation work for construction of underground facilities such as tunnels, subways, and pipelines for water and gas. The ability to ascertain the presence and accurately determine the location of highly contrasting stiff subsurface materials is thus important for site characterization.

Some options to estimate the mechanical properties of bedrock and overlying sediment include: 1) boreholes to establish subsurface stratigraphy coupled with downhole or crosshole seismic methods to acquire VS of layers, 2) seismic refraction data and analyses, and 3) surface-wave data and analyses.

o Boreholes provide access for understanding stratification of materials below the ground at discrete locations. Direct VS measurements can be obtained using downhole and crosshole seismic methods, but VS measurements of samples taken

1

from the borehole may not provide reliable values if the in-situ conditions cannot be replicated in the laboratory. Further, borehole measurements might not be practical when the site characterization is required over a large area or to great depth.

o The seismic refraction method is a non-invasive method to characterize the site by utilizing the propagation of seismic waves. A drawback of this method is ineffectiveness in detecting the presence of a soft deposit under a stiff deposit.

o The surface-wave method is another non-invasive technique which provides information of VSs from the near subsurface. This method is suitable in detecting the presence of a soft deposit under a stiff deposit which is an advantage over the seismic refraction method.

This thesis focuses on the surface wave method for characterization of a site having shallow bedrock that is defined by a sudden increase in stiffness at a depth of less than 10 m. The remainder of this introduction summarizes the current technology of surface wave methods and identifies several current problems that are addressed in the body of the thesis.

1.2 Review of the development, current status and challenges of surface wave methods

The propagation of surface waves in the subsurface layers of sediments can be used to estimate the VSs of the layers and to infer engineering behavior. The ability of the surface wave method to accurately characterize a site depends upon the type of source of seismic waves, specifications of geophones used to measure the seismic waves, field configuration of the sensors, the data-recording equipment and the analysis techniques. The following section briefly describes current Rayleigh-type surface-wave methods and challenges in applying them to shallow bedrock sites.

1.2.1 Using surface-wave methods

The surface wave method addressed in this thesis utilizes the dispersive nature of Rayleigh waves; this refers to how Rayleigh waves at different frequencies travel at different velocities in a layered medium. Fundamental-mode Rayleigh waves having high frequency (short wavelength) penetrate to shallow depths and provide information about the shallow subsurface; low-frequency (long-wavelength) waves penetrate to deeper depths and provide information regarding the deep subsurface (Figure 1.1).

A typical surface-wave procedure used to resolve a VS profile is as follows: 1) collect seismic data along a linear array of geophones installed on the ground surface; 2) transform the collected data from the time domain to the frequency domain in order to create a dispersion image, also known as an overtone image, which displays amplitude of wave velocity as a function of frequency; 3) from the overtone image, identify the dispersion curve (DC),which is the Rayleigh wave velocity as a function of frequency, for the fundamental mode; and 4) invert the fundamental-mode DC with an inversion process to produce a 1-D VS profile. In the inversion process, a forward model is applied to obtain a DC from a starting model, for which layer thicknesses as well as values of VS, Poisson's ratio, and density for each layer are assigned. Then, the starting model parameters are iteratively optimized to obtain a DC as similar as possible to the DC identified in the overtone image; the parameter set derived from the starting model in this fashion is known as the inverted profile. The inverted profile shows the estimation of the VS, Poisson's ratio and density with depths.

1.2.2 Multichannel surface-wave data collection and analysis

Section 1.2.1 outlined the four-step procedure for characterizing a site with a surface-wave method. After collecting and initial processing of surface wave data (Steps 1 and 2),

3

the critical third step is to determine the experimental DC from the overtone image. In this step, errors of obtaining the fundamental-mode DC will produce an erroneous VS profile for the site in Step 4. The surface-wave analysis for a shallow bedrock site produces fundamental mode and higher mode (called "multi-modal") DCs, which are explained in more detail below. Thus, correct identification of the multi-modal surface-wave DCs is critical in the data analysis process.

Surface-wave analyses of data from multiple geophones have been widely used for identifying the DCs of the fundamental mode and higher modes (Tokimatsu et al., 1992; Xia et al., 1999; Foti et al., 2003; Ryden and Park, 2004). Xia et al. (2000) and Beaty et al. (2002) presented cases where incorporation of higher modes along with the fundamental mode in the inversion process increased the accuracy of the inverted VS profile.

In the multichannel surface-wave method, geophones collect multichannel field records (time histories) of seismic signals generated from vibrating sources. The energy sources used in the surface-wave method can be broadly categorized into two types: active sources and passive sources. Active sources such as sledgehammers and weight drops produce relatively short wavelength seismic waves, and thus provide information regarding relatively shallow depths. In contrast, a Vibroseis is a type of active source that generates harmonic seismic signals of long wavelengths at relatively high energy levels, and therefore is useful to collect information from deeper depths (Luke et al., 2010). Vehicle movements ($\geq$ 3 Hz), atmospheric pressure changes (e.g., wind) ($\sim$ 1 Hz) and tidal motion (e.g., ocean swells) (< 1 Hz) are some examples of passive sources (Park et al., 2005). The seismic signals generated by these passive sources tend to have long wavelengths, and so are suitable for obtaining information regarding deeper depths.

4

Park et al. (1999) developed a multichannel analysis of surface waves (MASW) method that processes surface-wave data collected by a specified multiple-geophone array to obtain DCs. The authors demonstrated that the MASW method has the ability to take into account the complicated nature of seismic waves by separating unwanted noises such as body waves and scattered waves. These noises may adversely affect the analysis of the data. The MASW method uses a frequency-slowness transformation to obtain the fundamental-mode DC and also higher-mode DCs of the surface waves. Similar multichannel methods have also been used by other researchers including Malagnini (1996), Tselentis and Delis (1998), and Chik et al. (2009).

1.2.3 Challenges in the data collection in a common type of surface-wave method using sledgehammer or weight-drop

A common type of surface-wave method, conducted with a sledgehammer or an accelerated weight drop as a seismic source and 4.5 Hz resonant frequency geophones as signal receivers, can resolve a fundamental mode DC in a limited frequency band, around 13-50 Hz (e.g., Casto et al., 2009; Calderón-Macías and Luke, 2010). The low frequencies of the fundamental mode DC, which represent the deeper part of the profile, are missing in such a limited frequency band. This deficiency of the surface-wave data in the low frequencies can lead to non-unique solutions in the inversion process and reduce the accuracy of the resolved VS profile (e.g., Supranata, 2006; Hebeler and Rix, 2006).

Casto et al. (2009) studied the sensitivity of DCs to the VS of the bedrock by using a synthetic model that represented a shallow bedrock profile; they observed that the velocities in the DCs at low frequencies were sensitive to the VS of the bedrock. The authors observed cases in which insufficient data at low frequencies was the major reason for improper characterization of the depth and VS of bedrock.

5

1.3 High impedance-contrast boundary

1.3.1 Definition

A sequence of soft and unconsolidated deposits overlying bedrock at shallow depth represents a high-velocity halfspace (HVH) profile. The bedrock of an HVH profile has high impedance with respect to the material above the halfspace, where impedance is the product of density and velocity (e.g., Sheriff, 2002). A high impedance-contrast boundary (HICB) separates weak and low-VS material from stiff and high-VS material in the HVH profile.

1.3.2 Challenges due to an HICB

A reliable estimate of the VS of layers can be readily obtained from the fundamental-mode inversion of the surface waves for those sites whose stiffness and VS increase gradually with depth (e.g., Xia et al., 1999) as shown in Figure 1.2. But, the VS profile of a shallow bedrock site, which has a sudden increase of stiffness at shallow depth (nominally less than 10 m) (Figure 1.3) might be difficult to resolve because multiple-mode DCs are formed due to partitioning of the surface-wave energy to higher modes (e.g., Foti et al., 2003; Bergamo et al., 2011). The following four studies illustrate the challenges in using surface-wave methods to determine an accurate inverted VS profile due to the stiffness and velocity contrast posed by an HICB.

O'Neill and Matsuoka (2005) generated full-wave-field synthetic seismograms for VS profiles having an HICB. The authors studied two profiles, one having a low-velocity layer and another having a high-velocity layer at shallow depth. Both of these profiles have two HICBs. The first profile had a 4-m thick low-velocity layer that starts at 2 m depth. The VS of the low-velocity layer was 175 m/s, and the VS of each of the adjacent layers were 200 m/s. Similarly, the second profile had a high velocity layer that had

6

thickness of 4 m and VS of 200 m/s. The layers above and below the high velocity layer had the VS of 150 m/s and 175 m/s, respectively. The authors observed increase in the velocity at the same frequency in the apparent DC, which is a DC that represents the seismic energy contribution of all participating modes, in the overtone image and attributed this phenomenon to partitioning of the surface waves into higher modes. Similarly, Song et al. (2007) studied synthetic surface wave data for a profile which had a 1-m thick low velocity layer at 3 m depth. The VS of the low velocity layer was 150 m/s and the VS of the each of the adjacent layers was 200 m/s. The authors found higher modes in an overtone image which was developed from the analysis of the surface wave data.

Casto et al. (2010) studied the surface wave data collected in a shallow bedrock profile (less than 10 m) to characterize the site. The authors observed higher mode data along with the fundamental mode. This study is discussed in detail in this thesis.

Calderón-Macías and Luke (2010) studied a theoretical model that represented a shallow bedrock profile. The depth to the bedrock was 10 m, and the VS of the bedrock was 5 times the VS of the shallow layer. The authors observed the DCs of the fundamental mode and higher modes for the profile. The authors also studied the sensitivity of the multi-modal DCs to change in the VS of the layers. They noticed that higher-mode DCs are more sensitive to changes in the VS of the profile at depth than the fundamental-mode DCs in mid-range frequencies. They also found that higher-mode DCs are not always easy to distinguish from the fundamental mode DC and other scattered energy.

The average VS of the upper 30 m (Vs30) is adopted by ICC (2006) for seismic site classification and can be obtained from the surface wave method. Pitilakis et al. (2004)

7

observed that Vs30 measurements can be misleading for the classification of a site having shallow bedrock. The authors demonstrated that the too-high velocity of bedrock that resulted from a surface wave method can yield a Vs30 measurement that is too high; this may lead to an underestimation of site amplification.

1.3.3 Previous studies to resolve VS profiles having an HICB using surface waves

In Section 1.3.2, it was stated that higher mode DCs are formed due to presence of an HICB. Correct identification and interpretation of these DCs are required for the successful multi-modal inversion and estimation of the velocity of layers in a VS profile. The following researchers used multichannel data to produce dispersion images for which fundamental mode and higher modes were analyzed to resolve VS profiles for sites with HICBs.

Beaty et al. (2002) analyzed surface wave data collected at a site consisting of an approximately 10-m-thick layer of sandy and silty clay deposited over compacted glacial tills. The DCs of the fundamental mode and two higher modes were obtained in the frequency range of 10-80 Hz using a sledgehammer. The authors applied simulated annealing, a type of inversion method, to invert these multi-modal DCs, and to obtain the VS profile. The authors found that inversion of the fundamental mode by itself was not sufficient to resolve this profile where significant energy is partitioned to higher modes. The authors concluded that an improved reliability and low uncertainty in the resolved profile could be obtained by inverting the multi-modal DCs.

Bergamo et al. (2011) collected surface-wave data at a site consisting of a thin cover of soft soil over limestone bedrock. The data were collected using a 5-kg sledgehammer source and an array of 48 4.5-Hz vertical geophones with a spacing of 1 m. The apparent DCs were obtained with a frequency-wavenumber analysis implemented in Surface Wave

Analysis Torino (SWAT) software developed at Politecnico di Torino (Italy). The authors used a Monte Carlo algorithm, based on a multi-modal misfit function, for inversion of the apparent DCs. The apparent experimental DCs were fitted with theoretical DCs to resolve the profile. The resolved profile showed a high velocity contrast (the ratio of velocity of the bedrock to that of the layer was about 4.5) at a depth of 0.8 m, which indicates the presence of very shallow limestone bedrock.

Song et al. (2007) illustrated the advantages of incorporating higher mode DCs along with the fundamental mode DC to characterize a real site having a 1-m-thick low-velocity layer between the depths of 1.6 m to 2.6 m. The ratios of the velocity of the adjacent layers to the low-velocity layer were approximately equal to 2. After inverting only the fundamental mode data, they obtained an unrealistic VS profile. An accurate estimate of the VS profile was obtained with the inversion of the DCs of fundamental mode as well as higher modes.

The field study performed by Casto et al. (2009) involved collection of surface wave data from a site having a thin layer (<10 m) of unconsolidated clay residuum deposited over basaltic bedrock by using a 36-kg elastic weight drop as the seismic source and 24 4.5-Hz resonant frequency geophones spaced at 1.5 m. This shallow bedrock test provided motivation for this thesis, and is referred to repeatedly throughout the thesis. Both the seismic compression refraction method and MASW method were applied along the same survey line. A borehole situated approximately 10 m from the survey line showed the depth to bedrock was about 5.1 m. The seismic compression refraction test showed that the depth to bedrock was about 7.5 m, and compressional wave velocities of the layer and bedrock were in the range of 440-2000 m/s and 2400-5400 m/s, respectively. The authors assumed that the VS of the unconsolidated layer and bedrock

9

were 0.4 and 0.6 times the compressional wave velocities, respectively. This corresponds to Poisson's ratios of 0.40 and 0.22 for the layer and bedrock, respectively. The corresponding ranges of VS for the layer and bedrock are 176-800 m/s and 1440-3240 m/s, respectively. The authors analyzed the data with the Surfseis software (Kansas Geological Survey, 2006) and picked the fundamental-mode DC in the range 13-50 Hz. A starting model, assembled from the results of the seismic refraction, having 6 layers plus halfspace was used for the inversion test. The authors obtained a good fit of a theoretical DC with the experimental DC from the inversion. The VS profile, inverted using fundamental mode data only, showed a clear jump in velocity at the depth of 7.5 m. Based on the prior information and results of inversion, the authors concluded that the top of bedrock appeared at the depth of 7.5 m. Differences in the depth to bedrock obtained from lithological log and seismic tests might be due to lateral variability. The inverted profile showed the VS of unconsolidated material and bedrock were in the range of 180-657 m/s and 2163-2175 m/s, respectively. These were within the range of expected velocities. The authors concluded that in using the common type of surface wave method a credible VS profile for the shallow bedrock site could be resolved providing that, relevant prior information is available. The authors also conducted synthetic studies which demonstrated that confidence in inverting for the depth and the VS of the bedrock would be enhanced by expanding the analyses to include higher mode dispersion data that appear within the sampled frequency band.

Similarly, Foti et al. (2003) demonstrated the advantage of seismic refraction data as prior information for developing a starting model. The authors also concluded that the introduction of prior information would be needed in mitigating the problem of non-uniqueness in the solution of surface-wave inversion.

Wood (2009), on the other hand, demonstrated that a site with an HICB can be characterized with a fundamental-mode inversion alone by optimizing the field setup. The author studied a site in northwest Arkansas that consisted of soft sediment over a stiff limestone formation. The MASW method was applied to construct fundamental-mode DCs for the site. The author was successful in inverting the fundamental-mode DCs to characterize the site profile; the profile was verified by seismic borehole surveys. The average depth to the HICB from the MASW method and seismic borehole survey were 5.5 and, 5.8 m, respectively. But, the lithological log showed the depth of the limestone formation at depth of 7.5 m. According to the authors, the discrepancy in the depth by seismic methods and lithological log might be due to lateral variability in the limestone formation. The authors suggested that the optimum field setup for characterization of an HVH profile similar to that of the studied site would be 24 4.5-Hz resonant frequency geophones spaced at 1 m and a Vibroseis source at the distance of 9 m away from the first geophone.

1.4 Research topics

The research presented in this thesis addresses the challenges discussed above. This includes 1) improving the ability to resolve 1-D VS profiles for a site containing an HICB, 2) demonstrating limitations on data processing and interpretation of a common type of surface wave method for the case of an HICB, and 3) providing guidance for data collection suitable for sites with HICBs. To achieve these goals, the research topic addressed is as follows: Estimating the depth and VS of shallow bedrock by utilizing multi-modal surface-wave data in a frequency band limited by practical considerations. To address this topic, the following subtopics are addressed:

11

i) Rough estimation of the depth to shallow bedrock for building a starting model from the collected surface-wave data in the absence of prior information about the site.

ii) The inversion of multi-mode DCs to resolve a VS profile for a shallow bedrock site, considering practical limitations in the frequency band that is resolved.

iii) Benefits of incorporating higher modes along with the fundamental mode in the inversion process for shallow bedrock sites.

iv) Some consequences of misinterpreting multi-modal surface-wave DCs in an overtone image for a shallow bedrock site.

1.5 Organization of the thesis

In order to characterize a shallow bedrock profile, having an early estimation of the depth to bedrock would improve the inversion process of the surface-wave method and would mitigate the non-uniqueness problem of the inversion. Chapter 2 proposes a method to roughly estimate the depth to the high-velocity halfspace using the estimated VS of the shallow subsurface and the shape of the fundamental-mode DC. This information can be used to build a good-quality starting model.

Partitioning of Rayleigh-wave energy to higher modes can occur in the presence of the HICB in the shallow bedrock profile. The common type of surface-wave method described previously results in a lack of data in the low frequencies which is the zone in which the fundamental mode is most sensitive to the VS of the bedrock. For a given frequency, higher mode data are more sensitive to stiffness of deeper parts of the profile than is the fundamental mode. These facts emphasize the potential value of utilizing the higher modes for characterizing a shallow bedrock profile, which is addressed using a synthetic study in Chapter 3.

12

Chapter 4 explores the benefits of simultaneous consideration of the fundamental mode along with the higher mode Rayleigh-type surface waves for resolving the depth and the VS of shallow bedrock using error surfaces. This chapter also demonstrates the possibility of non-unique results due to 1) the selection of inappropriate starting models, and 2) the consideration only of data in a limited frequency band for the process of inversion.

Chapter 5 demonstrates effects of incorporating multiple modes in inversion for estimating the VS profile for shallow bedrock sites. Theoretical studies and analyses of a real-world dataset are conducted, considering data in broad and in limited frequency ranges.

The different modes are difficult to identify in an overtone image for an HICB site, and lack of low-frequency data for the fundamental-mode DC from common surface-wave measurement techniques exacerbates the problem. Chapter 6 shows the consequences of misinterpreting the low-frequency portion of the first higher-mode DC as the fundamental mode for an example case.

Chapter 7 shows the summary of results from all studied topics and provides conclusive remarks regarding the use of higher mode Rayleigh-type surface waves to resolve the VS profile for the shallow bedrock site. This chapter also offers some topics for further research.
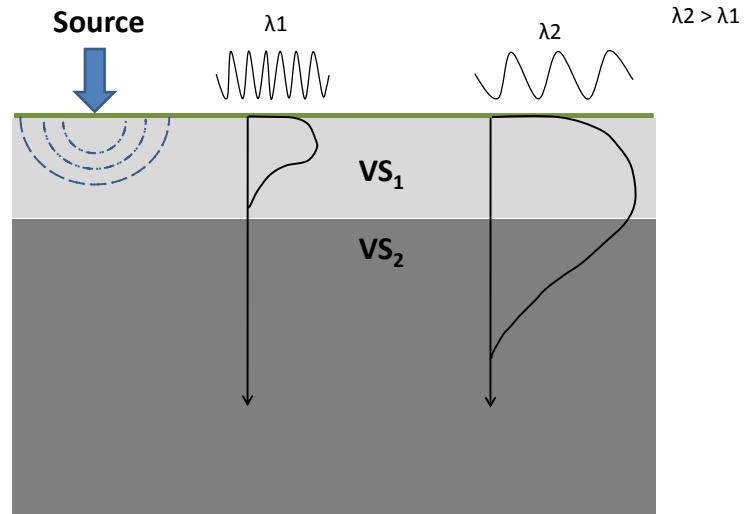
Figure 1.1. Generalization showing geometric dispersion of Rayleigh waves. The vertical displacement or depth of penetration of the wave is related to the wavelength. The wavelength of λ2 is longer than λ1.

$$VS_4 > VS_3 > VS_2 > VS_1$$
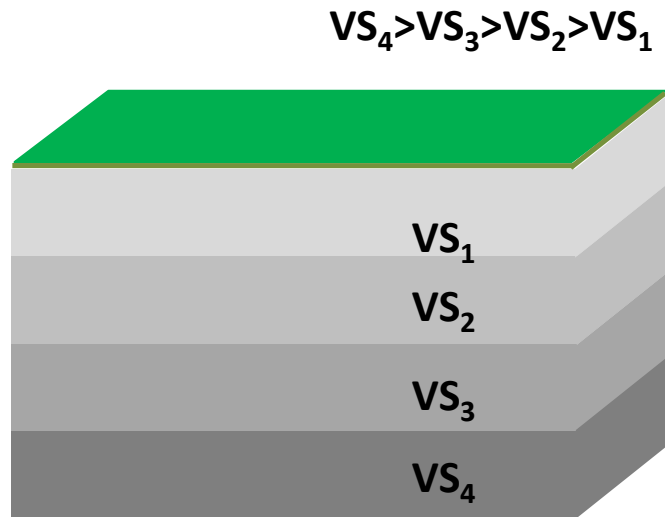
Figure 1.2. Schematic representation of a profile having shear stiffness of layers gradually increasing with depth.

14
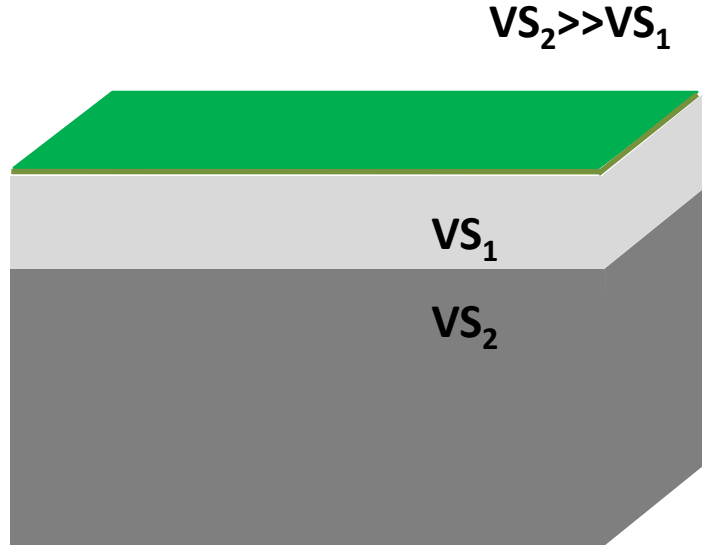
Figure 1.3. Schematic representation of an HVH profile.

CHAPTER 2

ESTIMATING DEPTH TO BEDROCK FROM THE RAYLEIGH WAVE

DISPERSION CURVE

2.1 Introduction

In some cases, independent information about the near surface of the site regarding layer geometry and expected material velocity can guide an inversion process to obtain a reasonable shear-wave velocity (VS) profile when it would otherwise not be possible (e.g., Luke and Calderón-Macías, 2007; Casto et al., 2009). Some examples of independent information are borehole logs, VS measurements from borehole-based methods, and seismic refraction data. In this chapter as in the rest of the thesis, the term "velocity" is used to refer to VS.

As stated earlier, a VS profile is developed from a dispersion curve (DC) through an inversion process which requires a starting model. The starting model consists of the layer geometry and VS as well as Poisson's ratio and density of the layers. In order to obtain a satisfactory solution in the inversion process, a starting model of good quality is sometimes required. It is common to invert for VS while leaving layer geometry and other parameters fixed. An informed selection of layer geometry reduces uncertainty in the solution of the inversion. For this study, a theoretical VS profile was considered that represents a shallow bedrock site which consists of a homogeneous sediment layer above bedrock. This system can be described as a high velocity halfspace (HVH) profile. Prior knowledge of approximate depth to bedrock facilitates the inversion process to converge to a meaningful solution (Calderón-Macías and Luke, 2010). In this chapter, a method is proposed for estimating the depth to bedrock by utilizing the shape of the fundamental mode DC and the expected VS of the overburden. The estimated depth is equivalent to

prior information for subsequent inversion of surface wave data. By providing the estimate for depth to bedrock, that is, the top of model halfspace, this process can be adopted to create a more robust starting model for the inversion.

2.2 A base model

In order to study the effects on the DC of the velocities of the layer and bedrock as well as the depth to bedrock, a forward modeling algorithm called Surface Wave Modal Inversion (SWAMI) coded by Rix and Lai (2005) was applied to generate the fundamental mode DCs from different VS profiles. In the base model selected for the study, the depth to halfspace was 2 m, and VS of the layer and halfspace were 200 m/s and 1700 m/s, respectively. Other parameters of the model were Poisson's ratio and density. Poisson's ratio for the layer and halfspace were assigned as 0.3 and 0.25, respectively. Density of the layer and halfspace were considered as 1700 kg/m^3 and 2200 kg/m^3, respectively. These DCs were computed over the range between 0 and 160 Hz. Figure 2.1 shows the fundamental mode DC for the base model. The DCs in most chapters of this thesis are plotted in the conventional manner, as velocity versus frequency. In this chapter, however, DCs are plotted as velocity versus wavelength. Recall that velocity is equal to the product of frequency and wavelength. This relation was used to transfer the plot from frequency-based to wavelength-based. Two bends are observed in the DC, characterized by their points of maximum curvature, one at a relatively short wavelength and the other at a longer wavelength. These points represent endpoints for the transition stage between the sections of the curve that become asymptotic to the Rayleigh wave velocities of the layer and the bedrock. These points of maximum curvature, which were identified visually, are referred to as the lower bend and upper bend, respective of velocity.

17

2.3 Test on the base model

Sensitivity studies were performed on the base model to understand the sensitivity of the bends to changes in the depth to bedrock as well as the velocities of the layer and the bedrock.

2.3.1 Changes in the depth to bedrock

Figure 2.2 shows a set of DCs developed after increasing the depth to bedrock from 2 m to 10 m in five steps at intervals of 2 m. Other properties of the base model are held constant. The changes in the depth to bedrock push forward the lower and upper bends along the wavelength axis. These results demonstrate that the two bends are equally sensitive to changes in the depth to bedrock.

2.3.2 Changes in the velocity of the layer

Figure 2.3 shows the changes in the DCs after varying the velocity of the layer from 200 m/s to 500 m/s in four steps at intervals of 100 m/s. Other properties of the base model are held constant. The lower bend thrusts upward -- in other words, the velocity increases -- at constant wavelength. However, only slight changes in velocity and wavelength are observed in the upper bend. In Figure 2.3, note that the lower bend of the DC for the highest layer velocity case is not developed fully. This occurs because observation of the DC is computed by frequency, which results in inconsistent data limits with respect to wavelength.

2.3.3 Changes in the velocity of bedrock

Figure 2.4 shows the changes in the DC after varying the velocity of bedrock from 1700 m/s to 2600 m/s in three steps at intervals of 600 m/s. Other properties of the base model are held constant. No change in the lower bend is observed. Only the upper bend thrusts upward as the velocity of bedrock increases. These results demonstrate that the

18

velocity of bedrock does not affect the lower bend. In Figure 2.4, the upper asymptotic end of the DC for highest velocity of halfspace case is not extended to the long wavelengths, due to early cut-off of DCs at the lower frequency.

2.4 General sensitivity studies

To explore a general method to estimate the depth to halfspace from the fundamental mode DC, a suite of sensitivity studies was conducted upon the model parameters. First, the depth to bedrock is increased from 2 m to 10 m for different velocities of bedrock, keeping the velocity of the layer constant at 200 m/s, as shown in Table 2.1 and Figure 2.5. As expected, the velocity of the bedrock has no effect on the lower bend. The relationship is approximately linear between the wavelength at which the lower bend occurs and the depth to bedrock. Figure 2.5 also shows that the linear fit worsens with increasing depth to bedrock. The same study is repeated for layer velocities of 500 and 800 m/s (Figure 2.6 and Figure 2.7; Table 2.2 and Table 2.3). The lower bends and upper bends tabulated in Table 2.1, Table 2.2 and Table 2.3 are observed from the DCs shown in Appendix A. These datasets consistently demonstrate that the wavelength at which the lower bend occurs is independent of the velocity of the bedrock. Figure 2.8 shows a summary of Figure 2.5, Figure 2.6, and Figure 2.7. This figure indicates that as the velocity of the layer increases, the slope of the line describing the wavelength at which the lower bend occurs with respect to depth to bedrock decreases. The coefficients of determination (R^2) of the lines in these figures are in the range of 97 % to 99 %, which implies a high reliability in representing the data points by those lines.

In the similar way, the wavelength at which upper bend occurs was also traced to explore patterns. Figure 2.9 shows the pattern of the wavelength at which the upper bend occurs when the halfspace velocity is at 2300 m/s. The upper bend shows a trend for

19

increasing wavelength at which the bend occurs, but it does not follow the pattern as closely as does the lower bend. The upper bend is surely more sensitive to the VS of the bedrock (halfspace) than it is to that of the layer.

The relationship of the slopes of the lines to the velocity of the layer provided in Figure 2.8 is shown in Figure 2.10. The relationship is quadratic with respect to the layer velocity. The equation of the curve is provided in Figure 2.10.

2.5 Estimating depth to halfspace

It is possible to estimate the depth to bedrock from the layer velocity and the wavelength at which the lower bend occurs. First, after assuming a suitable Poisson's ratio for the layer, the VS of the layer can be predicted from the asymptotic Rayleigh wave velocities at high frequencies. Consider that a DC represents the Rayleigh wave velocity of the material. The VS of the layer can be derived from the following relationship (e.g., Graff, 1975):

$$\frac{VS}{VR} \approx \frac{1+\upsilon}{0.87+1.12\upsilon}$$

where   VR = Rayleigh wave velocity and

   υ = Poisson's ratio

The ratio of VS to VR varies approximately from 1.11 to 1.07 for υ between 0.15 and 0.35. For a rough approximation, one might assume VS of the layer equal to VR at the high-frequency limit of the DC.

The depth to bedrock can be estimated by using the VS of the layer in Figure 2.10, and the observed wavelength at which the lower bend occurs.

In summary, the procedure to estimate the depth to bedrock includes two major steps:

20

(1) Estimating the VS of the layer and using it to find the slope of the line for the plot of "lower bend" versus "depth to bedrock" from Figure 2.10.

(2) Estimating the depth to bedrock from the observed wavelength at which the lower bend occurs divided by the slope.

2.6 Possible pitfalls of the method

The estimation of the depth to bedrock is based on the wavelength at which the lower bend occurs. Because the lower bend is identified visually, the selection of this point from the same DC can be different for each individual. This pitfall can be addressed through calibration.

Sometimes the lower bend does not appear in a DC due to lack of data at high frequencies. This data gap can be checked and possibly remedied in the field. An overburden layer having significant gradient in VS with depth might not yield a DC with a high frequency asymptote. Identification of the lower bend in this case may be challenging.

2.7 Application

This algorithm is tested with the experimental dataset which is discussed in chapter 5.

Table 2.1. The wavelengths at which the lower bend and upper bend occur as a function of depth to bedrock. The velocity of the layer is kept constant at 200 m/s.

Velocity of bedrock (m/s)	Depth to bedrock (m)	Wavelength	
		lower bend (m)	upper bend (m)
1700	2	4.6	65.6
	4	9.7	131.1
	6	13.8	209.0
	8	17.6	295.0
	10	24.0	369.0
2300	2	4.6	90.7
	4	9.7	181.2
	6	13.8	288.0
	8	17.6	406.0
	10	24.0	507.0
2900	2	4.6	129.4
	4	9.7	231.5
	6	13.8	367.0
	8	17.6	516.0
	10	24.0	645.0

22

Table 2.2. The wavelengths at which the lower bend and upper bend occur as a function of depth to bedrock. The velocity of the layer is kept constant at 500 m/s.

Velocity of bedrock (m/s)	Depth to bedrock (m)	Wavelength	
		lower bend (m)	upper bend (m)
1700	2	3.6	36.0
	4	7.3	72.0
	6	12.2	149.0
	8	14.5	145.0
	10	20.3	158.0
2300	2	3.6	50.0
	4	7.3	100.0
	6	12.2	203.0
	8	14.5	199.0
	10	20.3	288.0
2900	2	3.6	64.0
	4	7.3	127.0
	6	12.2	258.0
	8	14.5	254.0
	10	20.3	520.0

23

Table 2.3. The wavelengths at which the lower bend and upper bend occur as a function of depth to bedrock. The velocity of the layer is kept constant at 800 m/s.

Velocity of bedrock (m/s)	Depth to bedrock (m)	Wavelength	
		lower bend (m)	upper bend (m)
	2	3.0	18.0
	4	5.5	24.0
1700	6	10.0	50.0
	8	11.9	48.0
	10	14.5	88.5
	2	3.0	37.0
	4	5.5	43.0
2300	6	10.0	88.0
	8	11.9	100.0
	10	14.5	118.0
	2	3.0	70.0
	4	5.5	75.0
2900	6	10.0	132.0
	8	11.9	155.0
	10	14.5	150.0

24
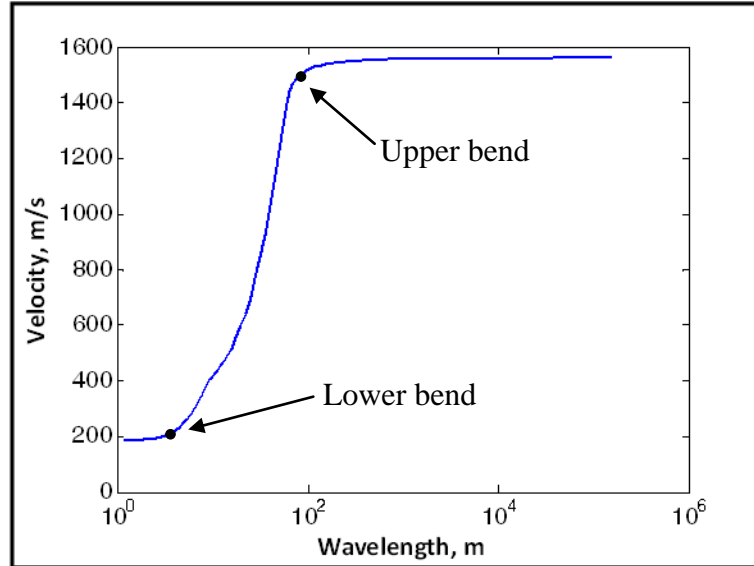
Figure 2.1. DC for the shallow bedrock profile ("base model") identifying the lower and upper bends.
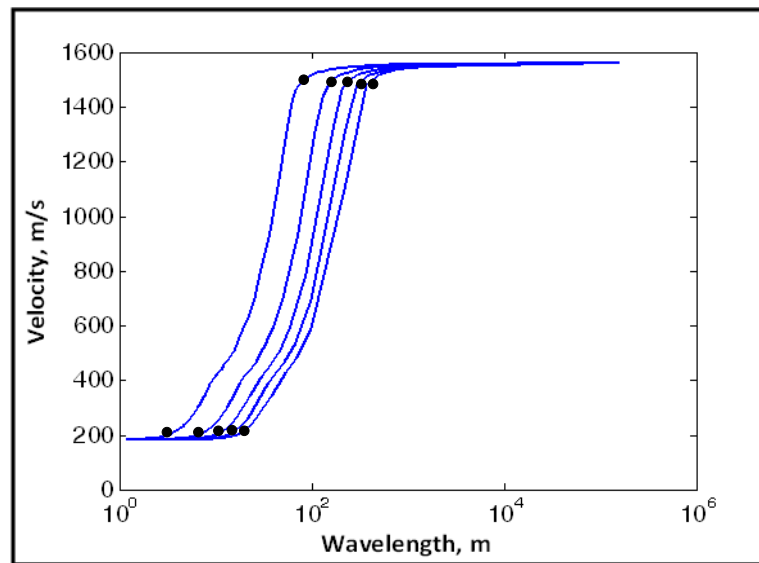
Figure 2.2. Set of DCs obtained when the depth to bedrock changes from 2 m to 10 m in increments of 2 m.

25
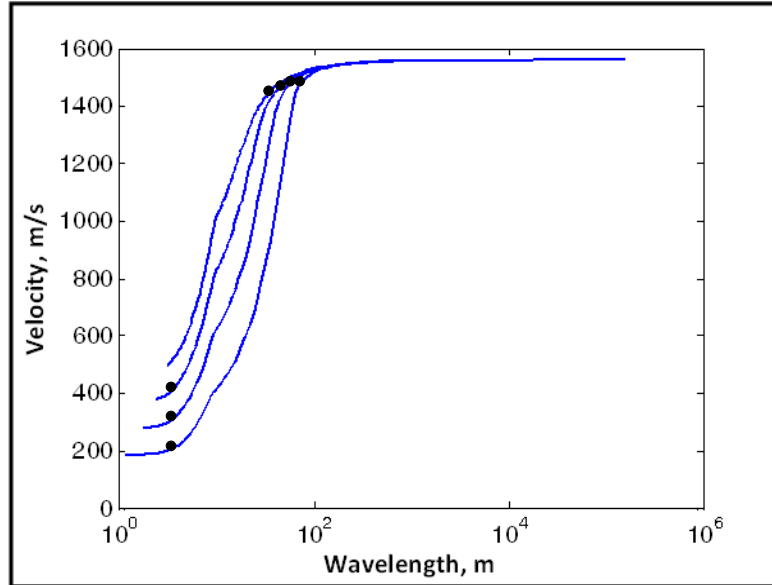
Figure 2.3. A set of DCs obtained when the velocity of the layer changes from 200 m/s to 500 m/s in increments of 100 m/s.
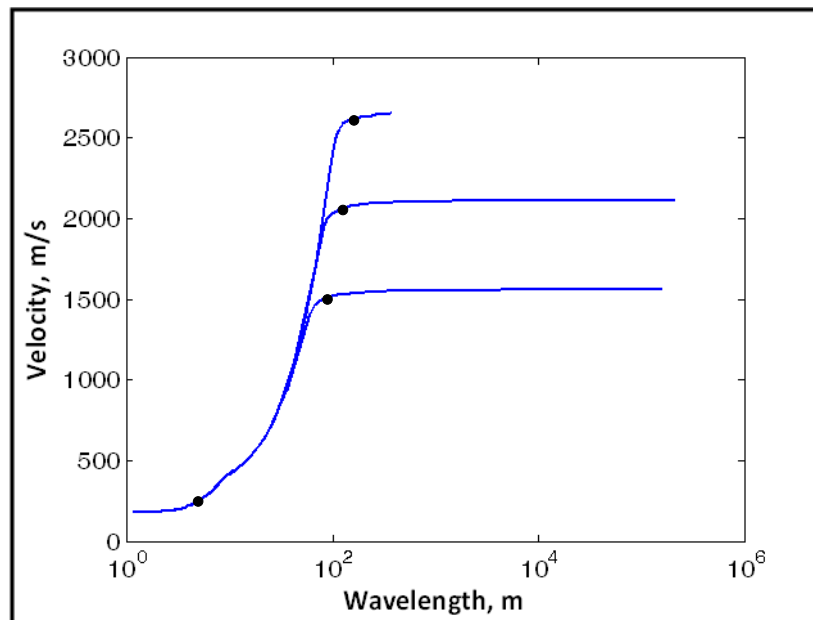
Figure 2.4. A set of DCs obtained when the velocity of bedrock changes from 1700 m/s to 2900 m/s in increments of 600 m/s.

26
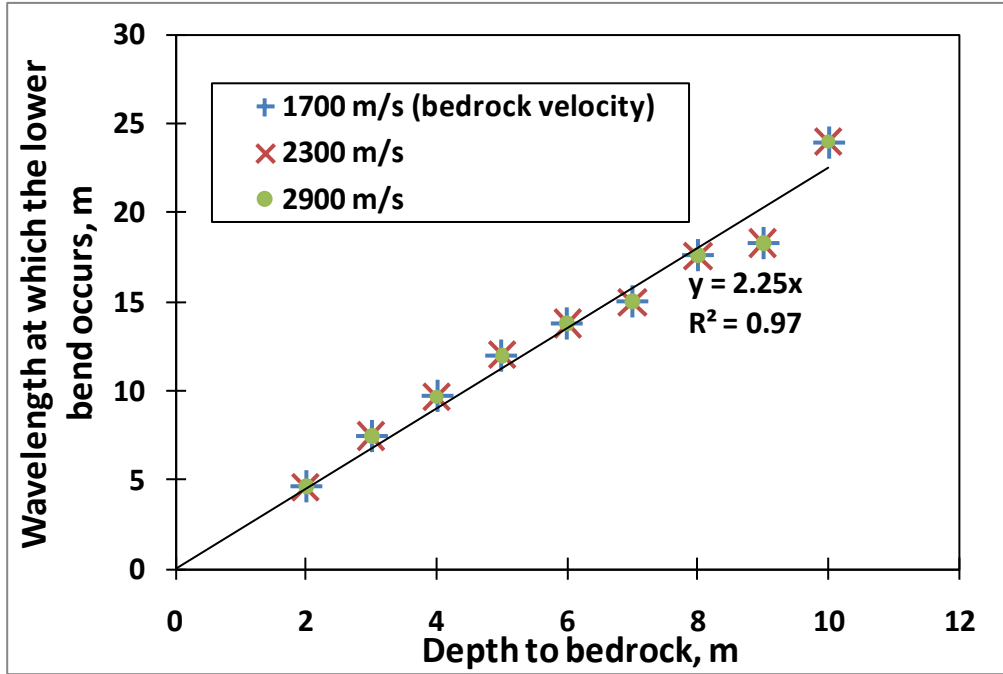
Figure 2.5. Variation in the location of lower bend with respect to depth to bedrock when the layer velocity is 200 m/s.
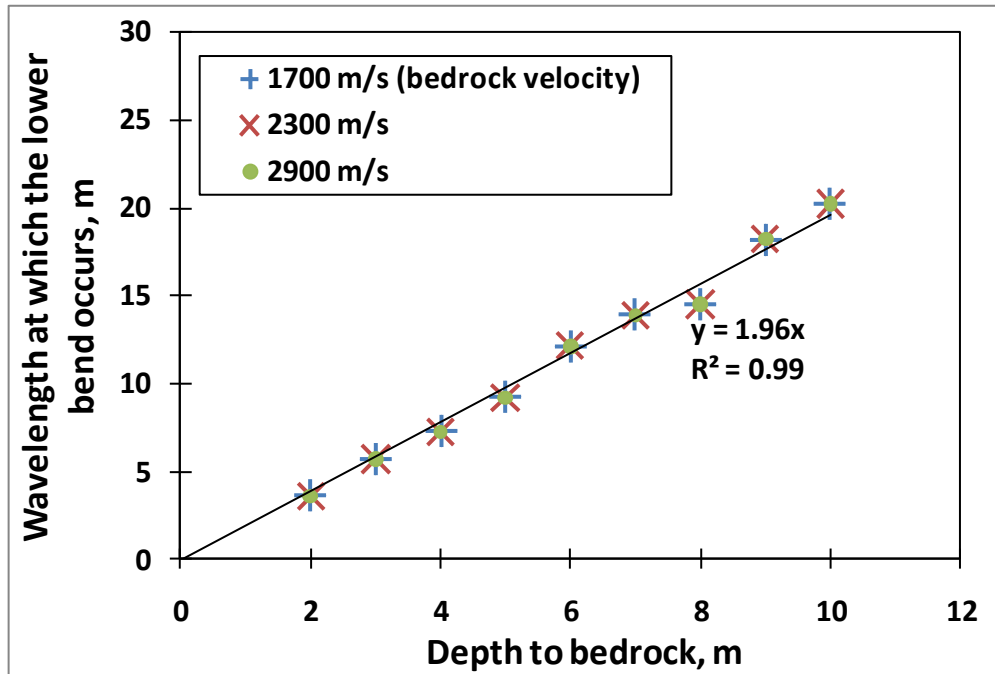
Figure 2.6. Variation in the lower bend with respect to depth to bedrock when the layer velocity is 500 m/s.

27
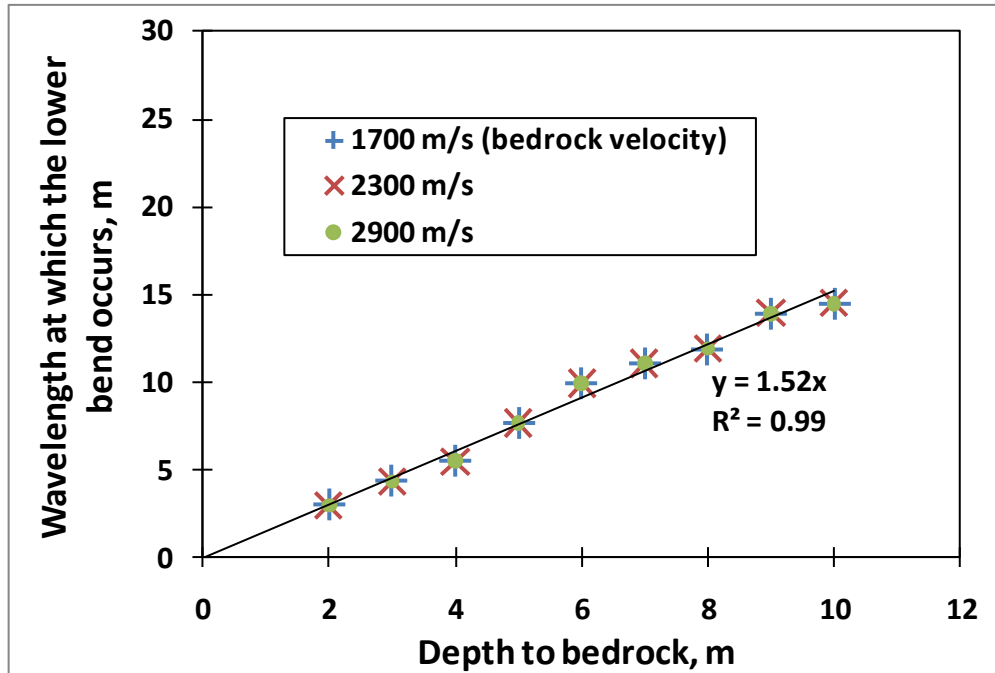
Figure 2.7. Variation in the location of lower bend with respect to depth to bedrock when the layer velocity is 800 m/s.
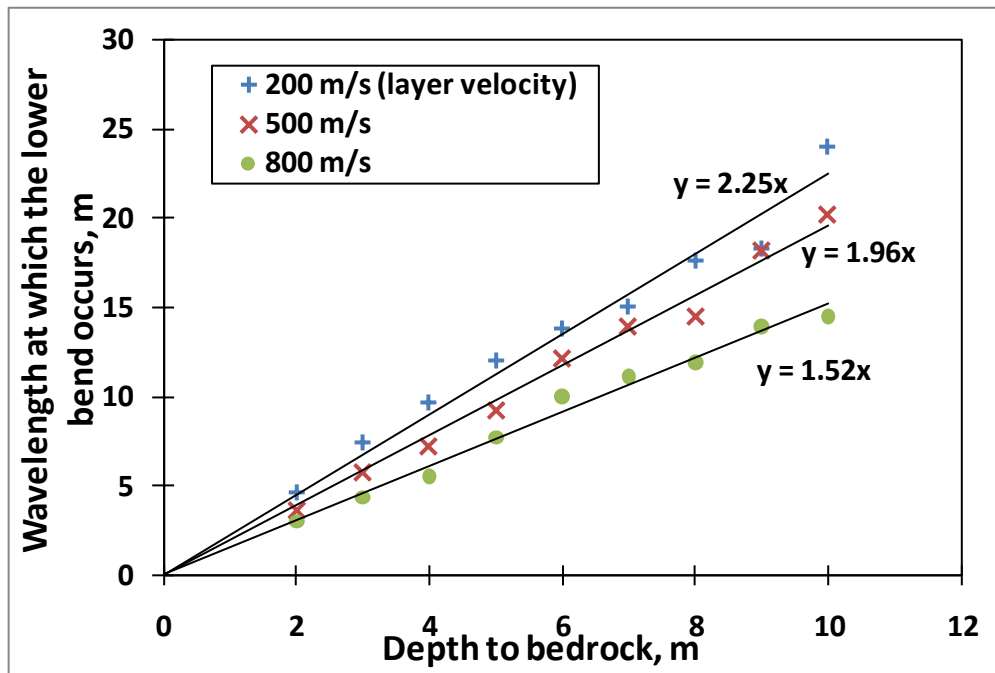
Figure 2.8. Variation in the location of the lower bend with respect to depth to bedrock when the layer velocity is 200 m/s, 500 m/s, and 800 m/s.
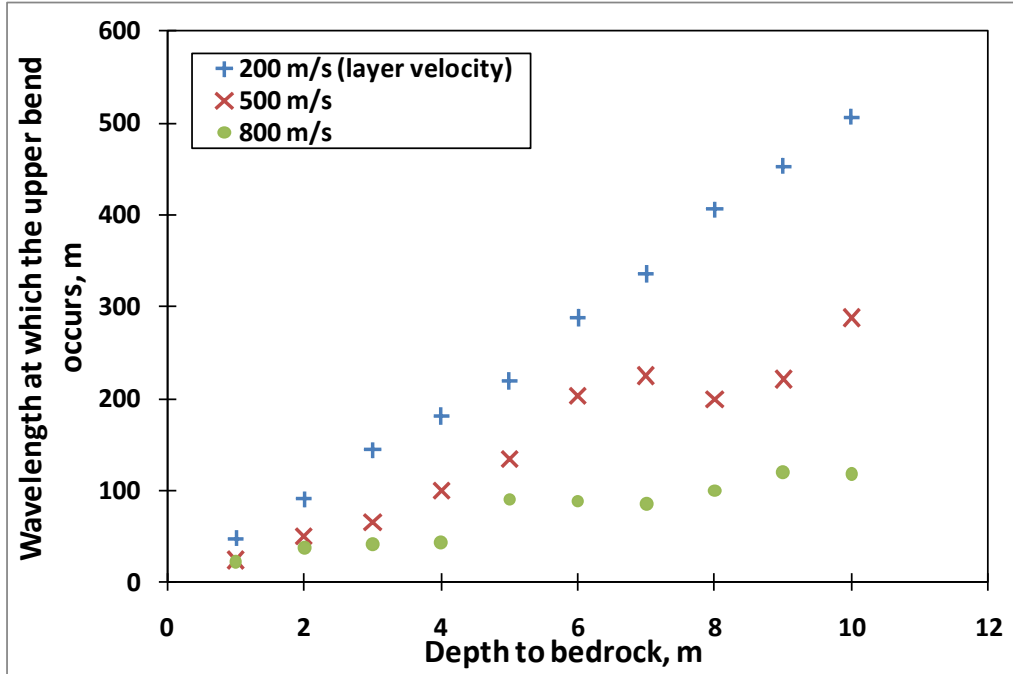
Figure 2.9. Variation in the location of the upper bend with respect to depth to bedrock when the halfspace velocity is 2300 m/s.

$$y = -8E\text{-}07x^2 - 0.0004x + 2.3587$$
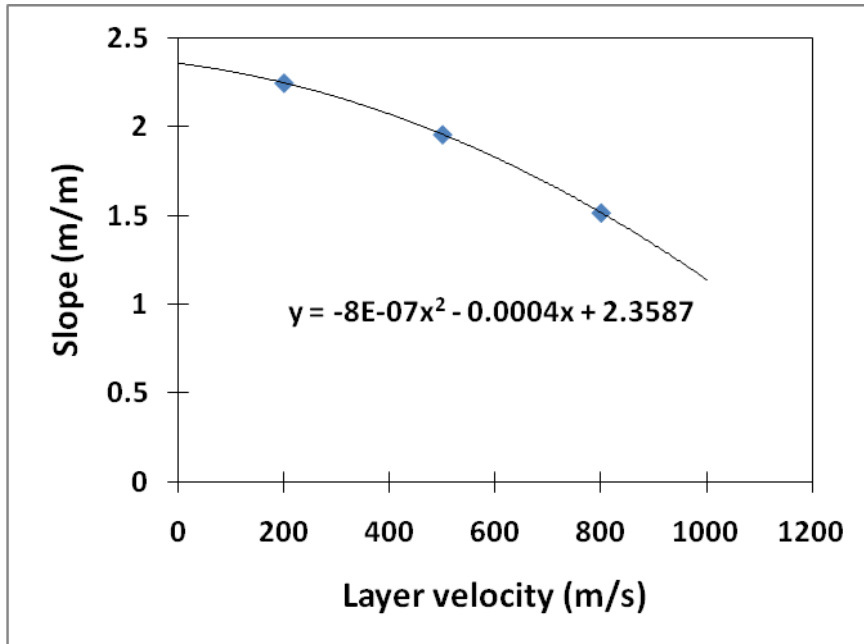
Figure 2.10. Quadratic relation of the slope of the line describing depth to bedrock versus wavelength at which lower bend occurs, with respect to the layer velocity.

29

www.manaraa.com

CHAPTER 3

LIMITATION POSED BY THE SAMPLING WINDOW

3.1 Introduction

A high velocity halfspace (HVH) model can be used to represent a site with unconsolidated sediments deposited over shallow bedrock. This chapter describes a set of sensitivity studies of three model parameters, namely shear-wave velocity of the layer and halfspace and depth to the halfspace, to explore some challenges inherent in characterizing shallowly buried bedrock using Rayleigh-type surface waves.

This chapter is adapted from a manuscript by Tamrakar et al. (2011) published in the Proceedings of the 43rd Symposium on Engineering Geology and Geotechnical Engineering, March 23 – 25, 2011, Las Vegas, Nevada. Some text here is copied verbatim from the proceedings document which is not copyrighted.

3.2 Challenges in a shallow bedrock site

As discussed in Chapter 1, previous research has shown depth and shear-wave velocity (VS) of shallowly buried bedrock to be surprisingly challenging to resolve with common type of multi-channel surface wave method. For example, in their shallow bedrock study, as shown in Chapter 2, Casto et al. (2009) observed deficiency of the fundamental-mode dispersion data at low frequency, which is the portion of that dataset that provides the information of depth and VS of the bedrock. The authors used synthetic data to demonstrate that higher modes might be useful to better characterize the site. Additional studies about the usefulness of the higher modes for a site with a strong velocity contrast at shallow depth have been conducted by other researchers including O'Neill and Matsuoka (2005) and Beaty et al. (2002). Both of these research teams

30

concluded that incorporation of higher mode data in the inversion process improved accuracy of inverted VS profiles.

3.3 A base model

The model parameters were tested in a sensitivity study to understand the ability of the dispersion curve (DC) to resolve a VS profile under normal field conditions. The baseline case is similar to the base model presented in Chapter 2 (Section 2.2). The layer has VS of 200 m/s and thickness of 2.5 m. The DCs were computed for models having VS of the halfspace ranging from 1700 to 2900 m/s in four steps at the interval of 400 m/s. The velocity contrast (ratio) between halfspace and layer was quite large in every case, ranging from 8.5 to 14.5. Poisson's ratio for the layer and halfspace were assigned as 0.3 and 0.25, respectively. Density of the layer and halfspace were considered as 1700 kg/m^3 and 2200 kg/m^3, respectively. Both Poisson's ratio and density were held constant during the study. The DCs for the fundamental mode and three higher modes were computed using SWAMI (Rix and Lai, 2005). As observed in Chapter 2, the low-frequency end of the computed DC will asymptotically approach the Rayleigh wave velocity of the bedrock, and similarly, the high-frequency end will asymptotically approach the Rayleigh wave velocity of the layer. Only the portion of the DC that falls between 13 and 50 Hz was considered, in order to model a frequency range which might be collected using typical active-source equipment and standard practices (e.g. Casto et al., 2009; Calderón-Macías and Luke, 2010). This frequency band is referred to here as the sampling window. Only if the asymptotic arms of the DC fall within the sampling window can we have confidence that a reasonably accurate VS profile of the system can be resolved from the dispersion data.

3.4 Sensitivity Studies

31

The baseline case is presented in Figure 3.1a. The distinct differences between the four fundamental-mode DCs associated with the different VS values of bedrock are manifested within the sampling window, but only below 20 Hz. The high-frequency, low-velocity asymptote needed to characterize the VS of the overlying layer is well resolved within the sampling window. Results indicate that the VS profiles modeled should be recoverable with reasonable confidence by inverting the dispersion data within the sampling window using the fundamental-mode DC alone; the higher mode data would provide mostly redundant information.

The case presented in Figure 3.1b differs from the baseline case in that the layer thickness is increased to 9.5 m. Now the portion of the fundamental-mode DC that is sensitive to the velocity of the halfspace has shifted to lower frequencies, outside of the sampling window. Considering only the portion of the DC that is within the sampling window, the fundamental-mode curve alone is clearly insufficient to characterize the halfspace: the portions within the sampling window of four DCs representing otherwise identical models with different VS of halfspace are identical. The first-higher mode would be unsuccessful too; the second higher mode dispersion data would be required to properly characterize the halfspace. Alternatively, results could be improved by extending data capture to lower frequencies. This option is sometimes impractical in the field, perhaps requiring a different source that delivers high energy at low frequencies.

The case presented in Figure 3.1c differs from the baseline case in that the VS of the layer is increased to 800 m/s. Only the fundamental-mode DCs appear in the sampling window. Here, the data within the sampling window appear adequate to characterize the velocity of the halfspace if the thickness and VS of the layer were known, but the upper-frequency limit of the window is too low to allow the layer to be characterized properly.

32

A practical solution to this problem is to sample the fundamental-mode data to higher frequencies, which is relatively simple do in the field. Higher modes would not be useful in this case because the cut-off frequencies, which define the minimum frequencies at which higher modes exist, are higher than the maximum frequency being sampled in this test.

In summary, the sensitivity study showed that the ability of an idealized fundamental mode DC to capture key components of an HICB system within a given sampling window depends on both the VS of the layer and its thickness. For a fundamental mode DC that cannot be adequately characterized at low frequencies within a given sampling window, options include a) observing the data outside the sampling window, which would likely require modifications in testing equipment and/or configuration, and b) incorporating higher modes along with the fundamental mode, within the existing sampling window. Independent information about the site would be needed to guide a practitioner to design acquisition parameters that would ensure adequate sampling of data with respect to frequency.
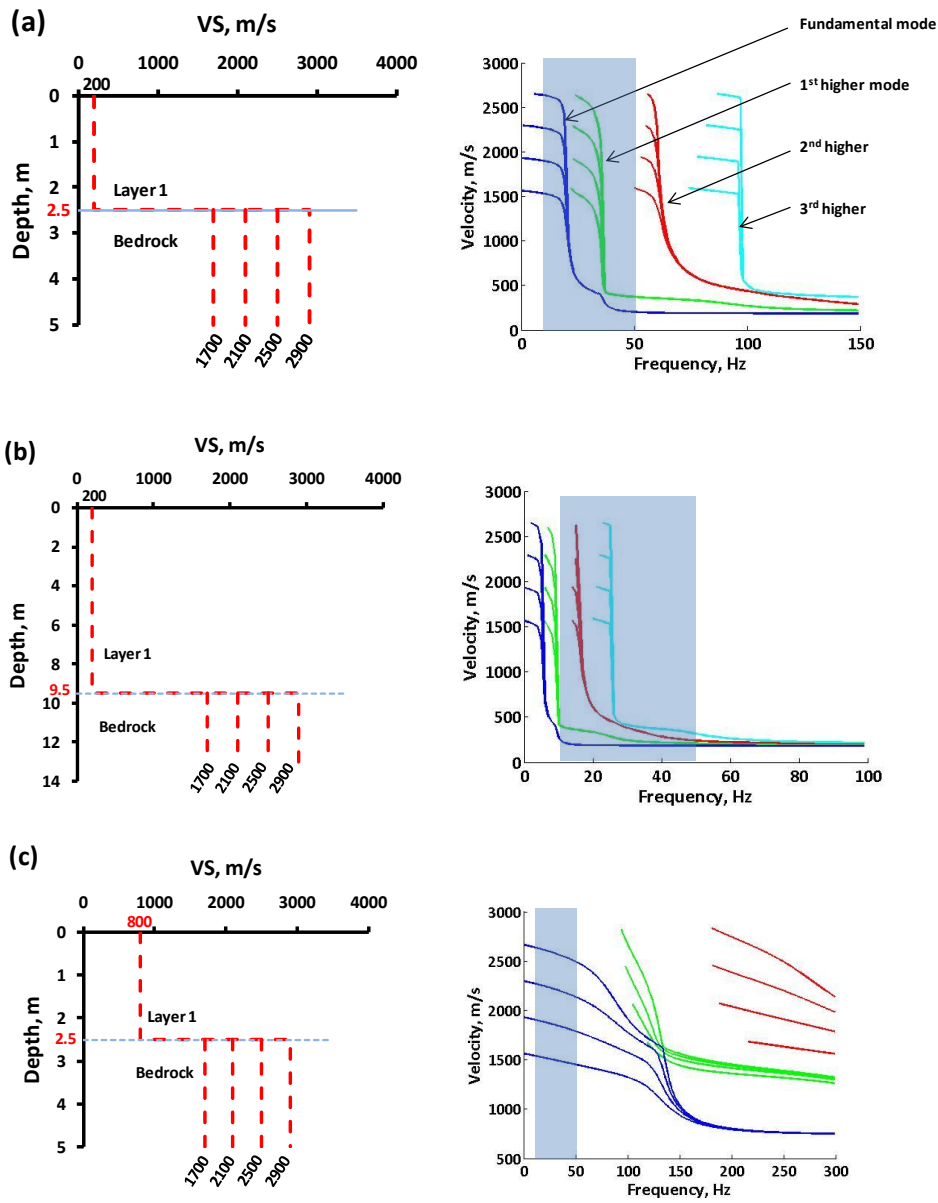
Figure 3.1 Synthetic dispersion curves for first four modes illustrating effect of modifying VS of halfspace: (a) upper layer 2.5-m thick with VS=200 m/s (baseline case); (b) upper layer 9.5-m thick with VS=200 m/s; (c) upper layer 2.5-m thick with VS=800 m/s. The sampling window is indicated by shading.

34

CHAPTER 4

INVESTIGATING THE HALFSPACE USING ERROR SURFACES

4.1 Introduction

In the common type of surface-wave method described previously, the fundamental-mode Rayleigh wave is inverted to resolve the shear-wave velocity (VS) profile. But a theoretical study on a shallow bedrock profile, also called a high velocity halfspace (HVH) profile, in Chapter 3 indicated that the fundamental-mode dispersion data is not sufficient to characterize such a profile in some cases, given practical testing limitations. Chapter 3 further illustrated that the higher mode data might be useful to resolve a shallow bedrock profile in some cases where fundamental mode data are insufficient. This chapter focuses on exploring the benefit of simultaneous consideration of the higher modes along with the fundamental mode in characterizing a shallow bedrock site.

To reliably estimate the VS profile from a surface-wave method, it is always desirable to select a good starting model for the inversion process. The good starting model consists of layer geometry and VS as well as Poisson's ratio and density of the layers that are close to the actual VS profile. Prior knowledge of site conditions is helpful for developing a good starting model (e.g., Calderón-Macías and Luke, 2010). This chapter further explores the importance of a good starting model in inversion.

To understand the importance of incorporating higher-mode data and selecting a good starting model for resolving a VS profile in the presence of a high impedance contrast boundary (HICB), Calderón-Macías and Luke (2010) used "root mean square (RMS) error surfaces" for synthetically computed DCs of the fundamental mode and four higher modes for an HVH profile. A brief discussion of this study is presented next, followed by a new study based on this work and performed on a real world dataset.

35

4.2 A RMS error surface plot

Calderón-Macías and Luke (2010) considered a base model representing an HVH profile in which the depth to the halfspace was 10 m and the velocities of the layer and halfspace were 300 and 1500 m/s, respectively. To study the importance of incorporating higher-mode data, the authors assembled a suite of VS profiles by varying two model parameters: (a) depth to halfspace and (b) VS of the halfspace. These parameters were discretized over the ranges 1 to 20 m and 400 to 2200 m/s, respectively. The DCs for those profiles were computed using the forward modeling code SWAMI (Rix and Lai, 2005), and the RMS difference between those DCs and the DC of the base model were calculated. Those RMS differences were plotted in a contour plot, known as an RMS error surface, which shows the depth to halfspace and VS of halfspace on the X- and Y-axes, respectively. One would have high confidence in ability to resolve the depth and VS of halfspace if the contrast is high in both directions, i.e., the plot has a clear single minimum.

The RMS error surface plots were studied over the frequency ranges of 0-50 Hz and 13-50 Hz (sampling window). The former case represents an ideal range of data collection that is not possible in the real situation. For this range, the gradient of the error surfaces for the fundamental mode was found to be high in all directions. Hence, the error plot was considered to have a good resolution and therefore, the fundamental mode was judged to be sufficient for the inversion process to converge to the true solution. Incorporation of all modes did not increase the resolution of the RMS error surfaces.

As mentioned previously, the latter case studied resembled a practical scenario for surface-wave studies with the use of a sledgehammer or accelerated weight-drop source, which lacks data in very low frequencies (e.g. Casto et al., 2009; Calderón-Macías and

36

Luke, 2010). The error surfaces for the fundamental mode indicated the possibility of satisfactorily resolving the depth to halfspace, but not the VS of the halfspace. The same observation was made for the first higher mode. The authors observed that incorporation of even higher mode DCs was required to adequately characterize the site within the sampling window. This case resembles that illustrated in Figure 3.1(b) of this thesis.

4.3 A real world dataset

The dataset of Casto et al. (2009) collected in a shallow bedrock site and discussed in Section 1.3.3 is referred to here for the synthetic study. To explore (1) the benefit of simultaneous consideration of the higher modes along with the fundamental mode in characterizing a shallow bedrock site and (2) the potential for success of different starting models to characterize the shallow bedrock site, error surfaces were computed and analyzed for the fundamental mode and four higher modes. Error surfaces were developed for the surface-wave data in a broad frequency range (0-120 Hz) and for a narrower the sampling window (13-50 Hz). The base model for developing the error surfaces was adopted from the results of seismic compressional refraction testing, as described in the next section.

4.4 Error surfaces

The HVH model, based on the shallow bedrock site discussed in Section 1.3.3 and shown in Figure 4.1, has a depth to halfspace of 7.5 m, and VS of the layer and halfspace of 400 m/s and 2200 m/s respectively. This model is considered as the base model in this chapter. The range of velocity of halfspace considered was equal to the estimate by Casto et al. (2009) presented in Section 1.3.3 that was derived from refraction data. As noted previously, there was discrepancy regarding the depth to bedrock observed from the seismic refraction test and from a nearby lithological log: the refraction test yielded depth

37

to bedrock as 7.5 m while the borehole log showed bedrock at 5.1 m. Considering all available information, error surfaces were created by varying the velocity of halfspace from 1400 m/s to 3000 m/s and the depth to halfspace from 5 m to 10 m, each in 51 steps. The "filled contour" graph function of Matlab software was used to develop the error surface plots from the computed RMS errors. Separate RMS error plots are created for each mode such that each plot represents the capability of an individual mode to independently resolve the depth and the velocity to halfspace.

4.4.1 Error surfaces for full frequency range

Figure 4.2 shows error surfaces for the fundamental mode and first four higher modes, considering the data from 0 to 120 Hz. The fundamental mode has uniformly low RMS error, so the contrast is low. This error surface shows approximately equal gradients along both axes leading to the minimum RMS error, which occurs at the center of the plot. Although the contrast of the RMS error is low, from the approximate symmetry of the plot, it seems the depth and velocity of halfspace can be resolved from the fundamental-mode inversion providing the search is sufficiently precise (Calderón-Macías and Luke, 2010).

The error surfaces for the higher modes show shapes elongated along the halfspace velocity axes. The elongation implies greater confidence in determining the depth to halfspace but greater uncertainty in determining the velocity of the halfspace, with respect to a circular surface. The RMS error surfaces of the third and fourth higher modes have high contrast relative to the other modes. These facts indicate that the depth to halfspace can be resolved with higher confidence from any of the higher modes than from the fundamental mode, and best with the highest mode. The elongated error surfaces display decreasing variability in contrast along the halfspace velocity axes with

38

increasing mode number. This implies increasing uncertainty in determining the velocity of halfspace with increasing mode number (Calderón-Macías and Luke, 2010). So for the common situation where layer geometry is fixed for inversion and VS is allowed to vary, in this case the incorporation of higher modes in the inversion would actually decrease resolution capability.

To further illustrate the contrasts, cross-sections along both axes of the error surfaces are shown in Figure 4.3 and Figure 4.4. The cross-sections a-a and b-b are drawn along the axes of the depth to halfspace and the VS of halfspace, respectively. These cross-sections are drawn along the center of the plots in both axes. In Figure 4.3, the gradient of cross-sections for the third and fourth higher modes is steeper than for the other modes. This fact implies that inversion of higher mode DCs, providing that they are free of noise and accurately characterized, allows us to improve our ability to resolve the depth to halfspace, when using the full frequency range (0-120 Hz). These cross-sections have similar gradients which means that higher mode DCs do not add any significant value in resolving the velocity of halfspace. So, for the case where a broad frequency spectrum is resolved, it can be concluded that the incorporation of higher modes would increase the capability of the inversion process to resolve the depth to halfspace but might have the opposite effect on resolution of the velocity of halfspace.

4.4.2 Error surfaces in a limited sampling window

The error surfaces in Figure 4.5 are created by considering only the data in the sampling window, that is, 13-50 Hz. The error surface of the fundamental mode in Figure 4.5 shows an elongated shape along the axis of halfspace velocity which is seen only in higher modes of Figure 4.2.

39

The error surfaces of the first and second higher modes show improvement in the gradients along both axes relative to the fundamental mode. The second higher mode is more improved than the first higher mode. So, these two modes might be useful for resolving the HVH profile for the case studied which uses a realistic sampling window.

The error surface for the third higher mode shows a uniform minimum RMS error region below the depth to halfspace at 7.5 m. A search that is started within this region will not converge to a correct solution in the inversion process because of uniformly low error in all directions. However, the region between 7.5 and 9.5 m depth shows a horizontally elongated error surface. This error region provides a better opportunity to estimate the velocity of halfspace compared to what was possible from other error surfaces. This fact implies that selection of a starting model having high depth to halfspace would permit the correct velocity of halfspace to be resolved. On the other hand, a starting model with low depth to halfspace would not deviate at all from the parameters of the starting model. So, the outcome from the use of the third higher mode depends strongly on choice of starting model.

For the fourth higher mode, zero RMS error is seen throughout the plot. This RMS error denotes the inability of the sampling window to capture any data for this mode.

To further illustrate the characteristic of the RMS error surfaces for third and fourth higher modes shown in Figure 4.5, three HVH profiles were considered with velocity of the layer and halfspace at 400 m/s and 2200 m/s, respectively. The depths to halfspace were assigned as 5.5, 7.5 and 9.5 m. Figure 4.6 shows third and fourth higher mode DCs for these three profiles, with the sampling window. Recall that the reference DC for the computation of the RMS error surface is obtained from the HVH profile having depth to halfspace 7.5 m. Figure 4.6 shows that only a small portion of the reference DC of the

40

third higher mode falls within the sampling window. Some low frequency data in the third higher mode DC for the profile with the depth to halfspace 9.5 m also falls within the sampling window. However, the DC of the profile with the depth to halfspace 5.5 m falls entirely outside the sampling window. So, the position of these DCs with respect to the sampling window explains the presence of uniformly minimum RMS errors for depth to halfspace less than or approximately equal to 7.5 m in the plot for the third higher mode in displayed Figure 4.5. The entire reference DC of the fourth higher mode falls outside the sampling window (Figure 4.6). So, the RMS error surface of the fourth higher mode in Figure 4.5 is completely flat.

Considering only the data in the limited sampling window, the fundamental mode error surface has low contrast and does not appear to be capable of resolving the velocity of halfspace (Figure 4.5). The higher modes, particularly first and second higher mode, have improved contrast. So, simultaneous consideration of the fundamental mode with the higher modes should produce a RMS plot with better contrast. However, higher modes are challenging to identify in practice, particularly for HICB cases, as will be addressed in Chapter 6.

To account for increased uncertainty in identifying higher modes, the concept of applying weighting factors to modes was considered for combined analysis of multi-modal data. When Beaty et al. (2002) inverted the fundamental mode and the first two higher modes, they gave a higher weighting factor to the fundamental mode and lesser weighting to the higher modes, explaining that the assignment of the weighting factor depends upon the relative proportion of energy among the modes. The same process of assigning weighting factor is considered in this chapter, although in Chapter 5 a different approach is taken.

41

The first plot in Figure 4.7 shows the RMS error surface using weighting factors of 0.75 and 0.25 for the fundamental mode and the first higher mode, respectively. Compared to the error surface for fundamental mode only (Figure 4.5), joint consideration of two modes shows improvement in resolving both parameters. The second plot in Figure 4.7 is developed using the weighting factors of 0.75, 0.15 and 0.10 for the fundamental mode, first higher and third higher modes, respectively. The simultaneous consideration of three modes with the weighting factors does not show improvement in resolving the velocity of halfspace with respect to the two-mode solution.

In summary, for the case studied, the fundamental mode DC appears to be sufficient to resolve the depth and the velocity of halfspace when the data are considered in a full frequency range. But, the consideration only of the data in the sampling window reduces ability to resolve the velocity of the halfspace from the fundamental mode. However, the RMS error surfaces of higher modes considered within the sampling window show the potential to significantly improve resolution of the depth to halfspace as well as slightly improve resolution of the velocity of halfspace. This study of error surfaces also demonstrates by example the importance of selecting a good quality starting model for an HVH profile in order to converge to a meaningful solution in the process of inversion.

42
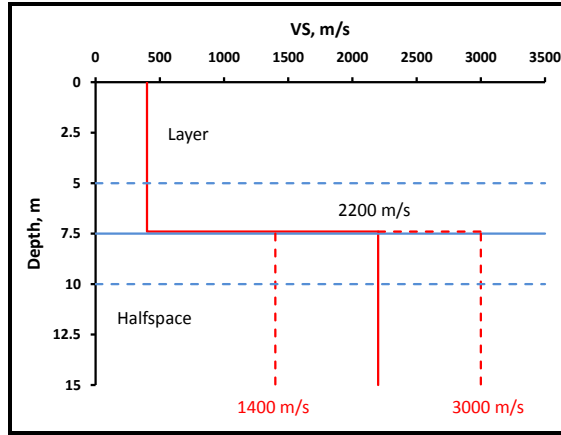
Figure 4.1. The base model is shown in the solid red line. The dashed lines denote the ranges of depth to halfspace and halfspace velocity explored to plot the RMS error surfaces.
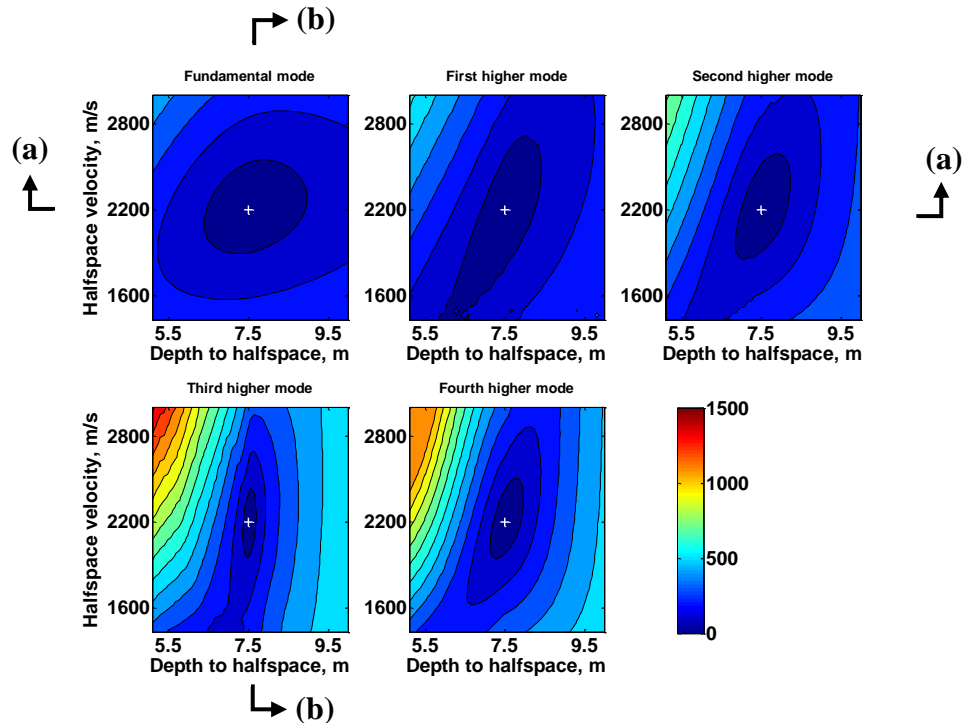
Figure 4.2. Error surface plots for HVH profile over the frequency range 0-120 Hz. The plots on the top, from left to right, are for the fundamental mode, first higher mode and third higher mode. Two plots in the bottom are for third and fourth higher modes. These plots show the RMS errors for different modes at the same scale. The plus sign "+" represents the correct solution.

43
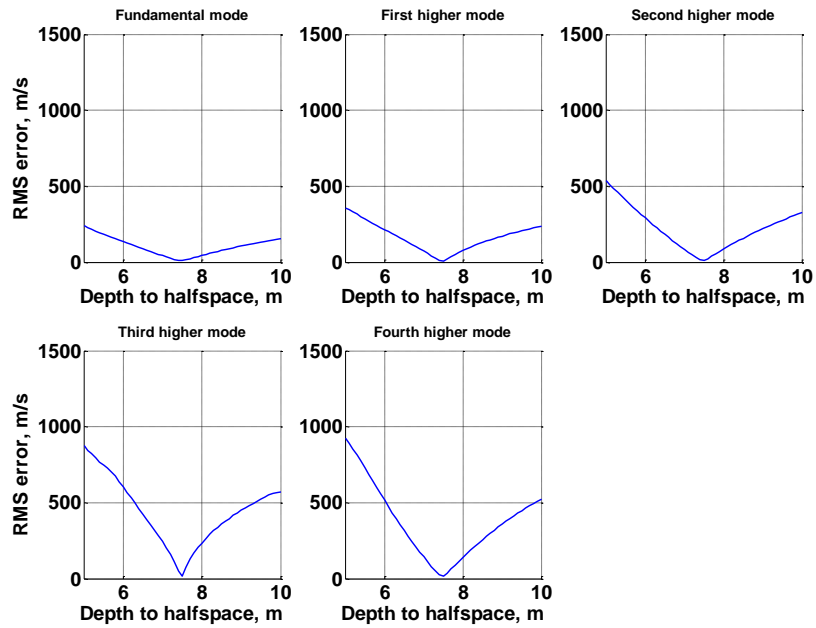
Figure 4.3. Cross-sections along a-a shown in Figure 4.2.
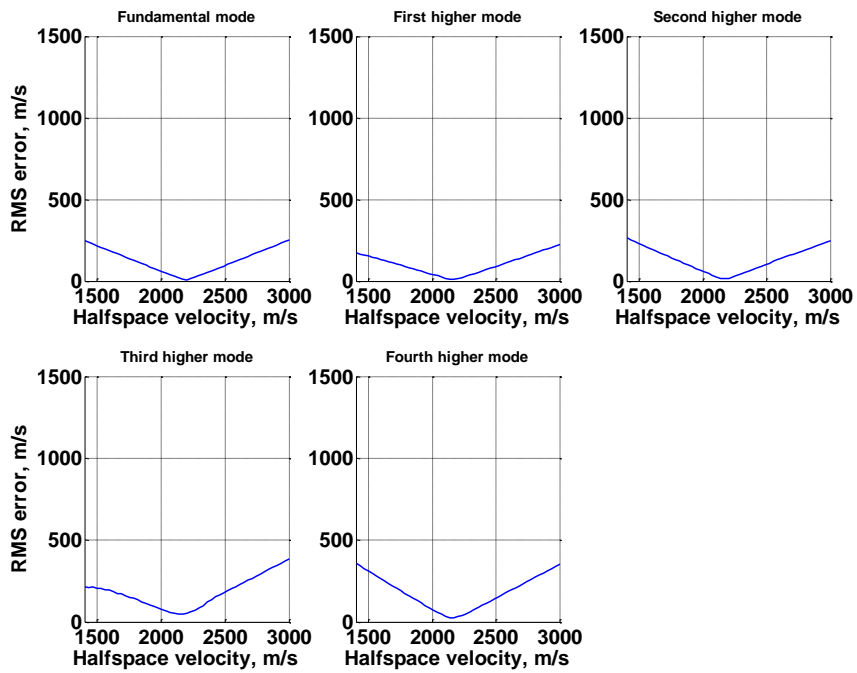
Figure 4.4. Cross-sections along b-b shown in Figure 4.2.

44
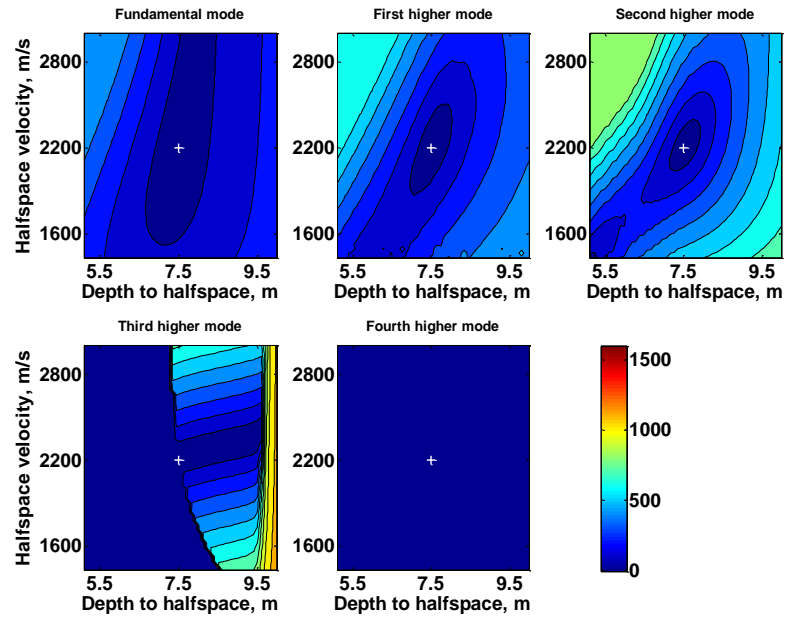
Figure 4.5. Error surface plots for HVH profile over the frequency range 13-50 Hz.
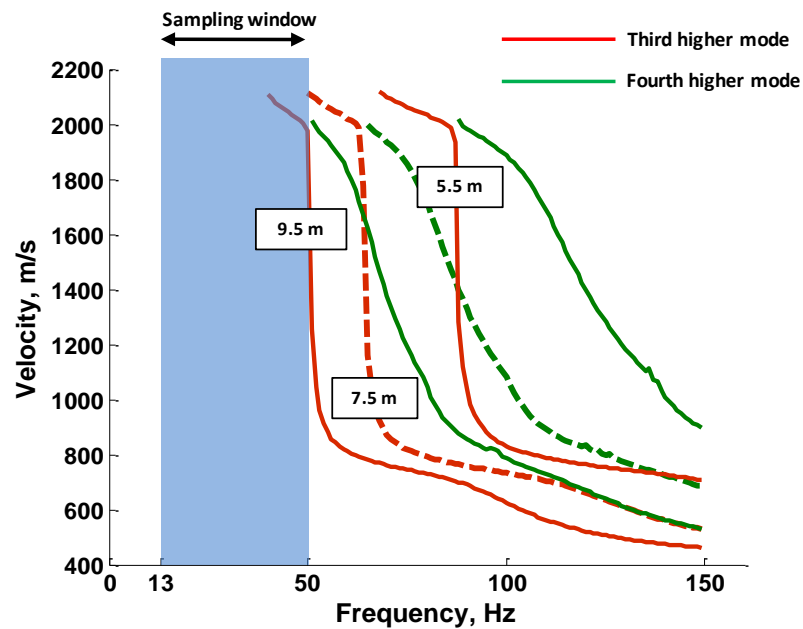
Figure 4.6. The third and fourth higher modes DCs for different depth to halfspace, noted on third higher mode curves. The velocities of the layer and halfspace are 400 and 2200 m/s, respectively.

45
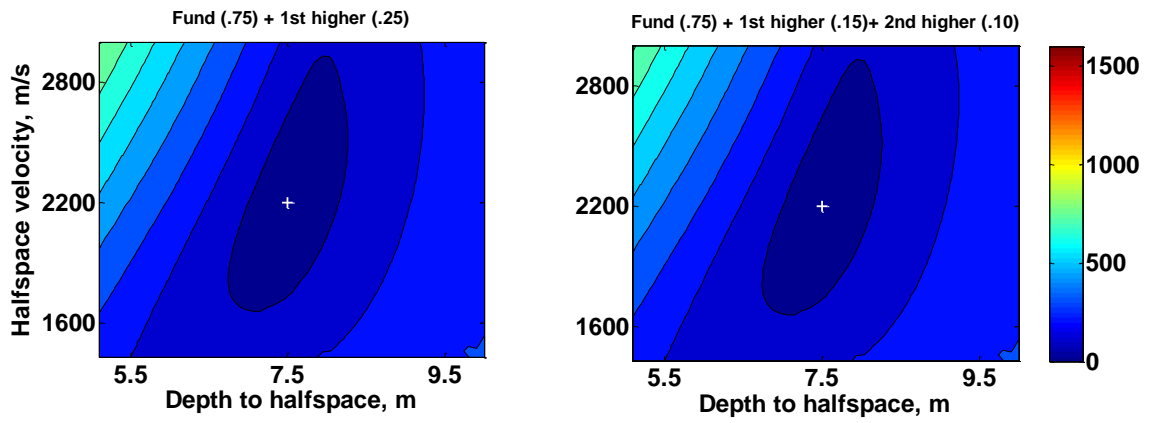
Figure 4.7. The error surfaces using different weighting factors for the fundamental mode and higher modes of HVH profile over the frequency 13-50 Hz.

CHAPTER 5

INVERSION OF MULTI-MODAL SYNTHETIC AND EXPERIMENTAL SURFACE

WAVE DATASETS FOR THE SHALLOW BEDROCK CASE

5.1 Introduction

This chapter contains investigations of higher mode Rayleigh-type surface waves to

characterize a shallow bedrock site using synthetic and experimental datasets.

5.2 Synthetic study

5.2.1 Synthetic dataset

The theoretical profile having a high impedance contrast boundary (HICB) at

shallow depth that was presented in Section 3.3 is considered as the target profile (Figure

5.1). The model parameters of the profile are shown in Table 5.1. The dispersion curves

(DCs) of the fundamental mode and first higher mode are developed over the frequency

range 2-80 Hz using the SWAMI code (Rix and Lai, 2005) as shown in Figure 5.1. These

DCs serve as the target for inversion. The target DCs were inverted without consideration

of any noise, and Poisson's ratio and density were held constant throughout the inversion.

During inversion, DCs were computed for two cases: for all observed data and then for a

limited frequency range of 20 – 60 Hz. The lower bound of the limited frequency range

was fixed just below the cut-off frequency of the first higher mode DC and lacked the

asymptotic part of the fundamental mode DC at low frequencies. One analysis in Chapter

3 showed this case where the component of the fundamental mode DC which represents

the bedrock is located outside the sampling window (Figure 3.1(b)). It was hypothesized

that the higher modes might be useful to characterize the shallow bedrock site in this

situation when the data at low frequencies of the fundamental mode DC are missing. So,

here, the data of the fundamental mode DC are limited in order to test the capability of the higher mode to resolve the shallow bedrock profile.

5.2.2 Inversion of dataset

The inversion of multi-modal surface-wave data was performed with two computer programs developed for the Applied Geophysics Center (AGC) at the University of Nevada Las Vegas. One uses a linearized least-square minimization process for optimizing the VS model and is referred to as Linearized Inversion (LI).The forward modeling algorithm used with this software is the SWAMI code (Rix and Lai, 2005). LI was developed by Carlos Calderón-Macías (Calderón-Macías and Luke, 2007). The other inversion software uses the stochastic optimization process of simulated annealing and is referred to as Simulated Annealing (SA). The forward modeling algorithm for this software is also SWAMI. The SA code was developed by Carlos Calderón-Macías for fundamental mode inversion (Calderón-Macías and Luke, 2007) and later modified by Xiaohui Jin for multi-modal inversion (Jin et al., 2009). Jin et al. (2009) used this multi-modal inversion software with fundamental mode and first higher mode Rayleigh-wave data to resolve a site containing a high velocity layer -- that is, a site with two HICBs. The program requires the user to specify search ranges of some model parameters. For this study, a profile of four layers plus halfspace was considered. Each layer is 1 m thick. The density and Poisson's ratio are the same as for the target profile. The search ranges of velocities assigned for the first, second, third and, fourth layers and halfspace are 100 to 600 m/s, 100 to 1200 m/s, 100 to 1200 m/s, 100 to 3000 m/s and 1000 to 3000 m/s, respectively.

Three different inversion processes were followed, as described in Figure 5.2. In the first process, LI was conducted using fundamental mode data and a simple,

48

straightforward starting model. In the second process, SA was conducted using the fundamental mode data to derive three VS profiles. An acceptance criterion was adopted such that residual error (Calderón-Macías and Luke, 2007) in every run must no larger than 30 % of the average residual error for the three runs. For any given test, the maximum number of SA runs that had to be conducted in order to obtain three acceptable outcomes was 5. The average of the three was used as a starting model for LI (Murvosh, 2011), again conducted using fundamental mode data only. The third process was identical to the second except that the inversion by SA was conducted using both the fundamental and first higher mode to derive the three VS profiles. Equal weighting of 0.5 was assigned to each mode, reflecting assumptions that (1) the two DCs are selected with equal confidence and (2) information to be gained from the higher mode is equally as important as the fundamental mode in resolving the profile.

5.2.3 Inversion with all observed data

5.2.3.1 Fundamental mode inversion with LI alone

Figure 5.3 shows the starting model for LI which was taken as the center of the search range specified for SA. Figure 5.3 also shows the inverted profile and corresponding theoretical DCs of fundamental mode and first higher mode. The fundamental mode DC results directly from LI. The first higher mode was computed using the SWAMI code with the resolved VS profile. This custom of computing the higher mode following inversion for fundamental mode only is repeated throughout this chapter. The fundamental mode DC is resolved well except over the frequency range 30-35 Hz where a kink appears in the target DC. The data of the first higher mode are resolved only above 38 Hz. The inverted VS profile recovers the correct VS of shallow layers above 2 m and

49

below 4 m. Velocity is excessively high, about 2000 m/s, in the third layer, and excessively low, 250 m/s, in the fourth.

5.2.3.2 Fundamental mode inversion with SA-LI

Three VS profiles were generated from three runs of SA applied to the fundamental mode. The inverted VS profiles and corresponding DCs are shown in Figure 5.4. The theoretical DCs show good fit with the target for both modes. The inverted VS values are similar to one another except for the fourth layer, just below the HICB of the target profile. The average of the three VS profiles (Figure 5.4) is close to the target profile. This profile is used as the starting model for LI which is conducted for the fundamental mode DC (Figure 5.5). The theoretical DCs from LI show near-perfect fit with the target for both modes although the final VS of the fourth layer is a poorer representation of the target than is the starting model.

5.2.3.3 Two-mode inversion with SA, followed by fundamental-mode-only inversion with LI

The process described in the previous section was repeated with the exception that inversion by SA sought matches to the DCs of both modes. The inverted VS profiles and corresponding DCs from SA are shown in Figure 5.6. Compared to the fundamental-mode-only inversion (Figure 5.4), misfit of the fundamental mode DC increases slightly over all frequencies, while the misfit of the first higher mode is not noticeably changed. Increased misfit in the fundamental mode DC is expected because of simultaneous consideration of two modes during inversion.

The average profile from SA, shown in Figure 5.6, is used as the starting model for LI which is conducted for the fundamental mode DC (Figure 5.7). Both theoretical DCs and

50

the inverted VS profile are nearly identical to those generated using the same process with fundamental mode alone (Figure 5.5).

In summary, the following observations can be made for this case when all observed data in a broad frequency range are considered for inversion. Fundamental mode inversion with LI conducted using a straightforward (uninformed) forward model was unsuccessful. However, fundamental mode inversion with SA-LI was successful. Two-mode inversion with SA followed by fundamental-mode inversion with LI and fundamental mode inversion with SA-LI resulted in identical solutions (Figure 5.8). In other words, the fundamental mode inversion is sufficient to predict the first higher mode accurately and therefore, higher modes would not be required to resolve the profile. In this case, the benefit of the higher modes would be only to check the results of the fundamental mode inversion. Next, we test whether consideration of data in a limited frequency band might require consideration of higher modes to properly characterize the site.

5.2.4 Inversion with limited data

The same process of inversion followed for all observed data, discussed in Section 5.2.3, is used here with data limited to the frequency range 20-60 Hz.

5.2.4.1 Fundamental mode inversion with LI alone

LI alone with limited data produces poor fits to the DCs and an unrealistic VS model, showing excessively high velocity at layer 2 and low velocity at layer 4 (Figure 5.9).

5.2.4.2 Fundamental mode inversion with SA-LI

Inversion of the fundamental mode with SA improved the fit of the DC significantly and resolved more realistic VS profiles (Figure 5.10) compared to the inversion with LI alone (Figure 5.9). Both modes of the DC are solved well except for the first higher mode

51

below 35 Hz. For a high velocity halfspace (HVH) profile, the low frequency portion of the DC is sensitive to the VS of halfspace (Calderón-Macías and Luke, 2010). The misfit of DCs in the low frequency portion of the first higher mode indicates that the deeper component (VS as well as thickness), particularly for the fourth layer, of the profile would need to be adjusted to obtain a satisfactory model. Here, the fourth layer might need some adjustments because the halfspace of the target profile starts just above this layer.

The LI process following fundamental-mode SA did not show much change in the VS model from SA (Figure 5.11). Misfit in the first higher mode DC for frequencies below 35 Hz is smaller but still significant.

5.2.4.3 Two-mode inversion with SA, followed by fundamental-mode-only inversion with LI

The consideration of two modes during inversion with SA (Figure 5.12) improves the fit of the DCs for the first higher mode compared to the fundamental-mode-only inversion with SA-LI, but reduces quality of fit for the fundamental mode (Figure 5.10). The three VS solutions are similar except for the fourth layer, as seen before, and to a lesser extent the third layer.

The LI process following SA resulted in improved fit of fundamental mode but increased misfit of the first higher mode below 35 Hz. The VS model is close to the target profile (Figure 5.13). Resolution of the fourth layer is greatly improved, although resolution of the halfspace is slightly reduced.

In summary, considering testing over a limited frequency range, the following four observations are made. First, as was seen for testing with the broader frequency range, the use of SA to build a well informed starting model significantly improved outcomes

with respect to LI conducted using a simpler, straightforward (uninformed) starting model. Second, inversion by SA addressing both modes followed by LI addressing only the fundamental mode yielded a reasonable fit to both DCs and a good VS model (Figure 5.13). Third, the multi-mode inversion with SA-LI improved the results with respect to fundamental-mode inversion with SA-LI to some extent. Fourth, VSs of halfspace resolved with LI and SA-LI are close to theVS of halfspace of the target profile (Figure 5.14).

5.3 Experimental study

5.3.1 Real-world-dataset

Similar studies are conducted using the surface-wave dataset collected at a shallow bedrock site by Casto et al. (2009) and described in Section 1.3.3.

The "normal" algorithm in the software Surfseis (Kansas Geological Survey, 2006) was used to create an overtone image and pick multi-modal DCs. The resolution of the image was adjusted to emphasize higher modes. Results are shown in Figure 5.15. In the figure, bands of relatively high amplitude can be observed that demonstrate the presence of the fundamental mode DC as well as at least three higher mode DCs. Scant evidence of a fourth higher mode is seen above the third higher mode, starting from the velocity of 500 m/s at 50 Hz.

The DCs of the fundamental mode and four higher modes were picked over the frequency range 12-50 Hz, as shown in Figure 5.16. These DCs are used for studying multi-modal inversion in this chapter.

In order to analyze multi-modal data, Casto et al. (2010) expanded their earlier study of the same surface-wave dataset (Casto et al., 2009). Casto et al. (2010) also produced an overtone image using the Surfseis software and picked multi-modal DCs. The DCs

53

picked by the authors are overprinted upon those picked for this study in Figure 5.17. The resolution of the overtone image developed by Casto et al. (2010) (not shown here) was quite different from that created for this study (Figure 5.15). For example, the overtone image by Casto et al. (2010) had poor resolution below 15 Hz. However, Figure 5.15 shows good resolution to about 12 Hz. Figure 5.17 shows that the DCs of the fundamental mode and first higher mode picked for this study are similar to those picked by Casto et al. (2010) except below 15 Hz, but the other higher modes are different.

5.3.2 Inversion of dataset

The same process of multi-modal inversion followed with the synthetic dataset was applied for the real-world-data as described in Figure 5.18. The starting model parameters and search range for SA were assigned after consulting prior information about the site discussed in Section 1.3.3.

The technique to determine the depth to halfspace that is discussed in Chapter 2 was applied in the velocity-wavelength plot for the fundamental mode for the experimental dataset. The VS and wavelength at which the lower bend occurs were observed to be 300 m/s and 17.5 m, respectively (Appendix B.1). Using Figure 2.10, the depth to halfspace was estimated at 8 m which is close to the depth of 7.5 m estimated from seismic compression refraction by Casto et al. (2010).

Here a profile is selected with three layers, each 2.5 m thick, plus halfspace. From prior information, the estimated ranges of VS for the layer and bedrock were 176-800 m/s and 1440-3240 m/s, respectively. So, the search ranges of velocity were assigned as 200 to 800 m/s for topmost two layers, 200 to 3200 m/s for other layers and 1400 to 3200 m/s for the halfspace. The layer geometry of the starting model allows the process to solve for

54

the halfspace depth indicated by the lithological well log, or by the seismic refraction test and the bend in the DC from the inversion process.

As mentioned in Section 4.4.2 and as will be illustrated in Chapter 6, identification and inversion of higher modes is a complex problem. For this study, the DCs of only the fundamental mode and first higher modes were considered.

5.3.3 Inversion with all observed data

When the full picked DCs were considered, unrealistic VS models resulted. To illustrate, the final results of SA-LI from fundamental mode and two-mode inversion are shown in Figure 5.19 and Figure 5.20, respectively. The supporting figures are not shown for brevity. The fundamental-mode DC fits are erratic. The VS profiles have unrealistically high velocity of halfspace. For the case when two modes are considered for SA, extreme velocity fluctuations are also observed. Chapter 6 of this thesis will demonstrate that such behavior might occur with an HVH profile when the DCs of the fundamental mode and first higher mode are misinterpreted at low frequencies. Therefore, the dispersion picks at low frequencies were disregarded and the inversion process was repeated.

5.3.4 Inversion with reduced dataset

The low frequency data of the fundamental mode and first higher mode were disregarded below 15.4 Hz and 17.8 Hz, respectively, following rationale discussed in Chapter 6 that dispersion curves for HICB sites are subject to misinterpretation at low frequencies, such that the first higher mode curve at low frequencies is appended to the fundamental mode curve at higher frequencies. The reduced dataset is shown in Figure 5.21.

5.3.4.1 Fundamental-mode-only inversion with LI

The direct application of LI on the limited data of the fundamental mode using the center of the search range as a starting model produced an erratic DCs and a VS model with unrealistically high velocity of the second layer (Figure 5.22). Surprisingly, the overall trend of the first higher mode fits well with the experimental data.

5.3.4.2 Fundamental mode inversion with SA-LI

Figure 5.23 shows the results of fundamental mode inversion with SA. The fundamental mode DCs are fairly close to the target DC for the most part. However, the first higher mode DCs are not. The three VS profiles are widely different in the bottom layer. The average of the three profiles gives a reasonable approximation of the expected two-layer system that fits anticipated velocity ranges. The depth to the HICB, 7.5 m, matches predictions from the refraction dataset and also the estimate based on the bend in the fundamental dispersion curve, following the method presented in Chapter 2.

The fit of the DC is improved by LI, also conducted using fundamental mode only (Figure 5.24), but the fit of the first higher mode remains poor. The reasonable solution obtained through SA is negatively affected by the LI process. Some unrealistic velocity fluctuation appears at layer 3. The HICB occurs at a greater depth than expected, and has VS slightly higher than the maximum expected velocity.

5.3.4.3 Two-mode inversion with SA, followed by fundamental mode inversion with LI

When the first higher mode is considered along with the fundamental mode for SA (Figure 5.25), an improved fit to the higher mode DC is observed, while the fundamental mode fit is degraded. Differences between the three VS profiles are smaller than with fundamental-mode only (compare Figure 5.25 to Figure 5.23). The average of the three profiles represents a two-layer system with velocities that are within expected bounds, but HICB occurs at a greater depth than expected

56

The fit on the fundamental mode DC is made nearly perfect by LI (for fundamental mode alone) following SA (Figure 5.26), but the fit for the first higher mode is poorer than some fits found in the SA process (Figure 5.25). The inverted VS profile is quite similar to its starting model (the average of three runs using SA for two modes) except for increased velocity fluctuation in layer 3.

In summary, considering testing with a reduced dataset, the following observations are made. First, the reduction of the dataset allowed for tractable solutions to be developed (DCs that are not erratic and generally follow the target), but only if an informed starting model was used. Second, both SA processes yielded credible VS profiles, although the two-mode solution placed the HICB lower than expected. Third, the LI inversion following SA in both cases yielded a less satisfactory solution than did the averages of three SA runs (which constituted the starting models for LI).

From this study of experimental data, it can be concluded that (1) the low frequency dispersion data in the overtone image might have been picked incorrectly. The tests did not indicate conclusively whether the incorporation of higher modes in inversion improved ability to estimate a reasonable VS profile. However, improving the fit to the fundamental mode DC by way of LI clearly did not improve the quality of the VS profile.

An interesting follow-on inversion test would be to cut one more data points from the low-frequency end of the experimental dataset for fundamental mode, which would shift still more heavily the burden of resolving the bedrock to the first higher mode data. It would also be instructive to test the picked multi-mode DCs using an LI algorithm that optimizes for multiple modes. And it would be interesting to conduct a statistically significant number of trials with SA in order to test whether the average of three runs is a viable representation (e.g., Luke and Calderón-Macías, 2007).

Table 5.1. Model parameters for the target profile.

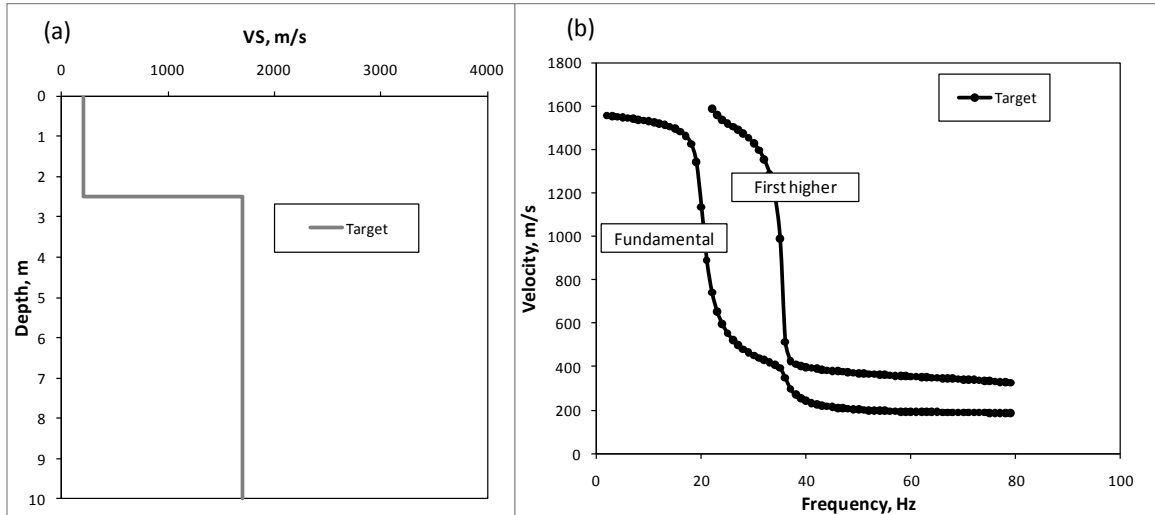| Velocity (m/s)	Poisson's ratio	Layer thickness (m)	Density (kg/m^3)
200	0.30	2.5	1700
1700	0.25	NA	2200

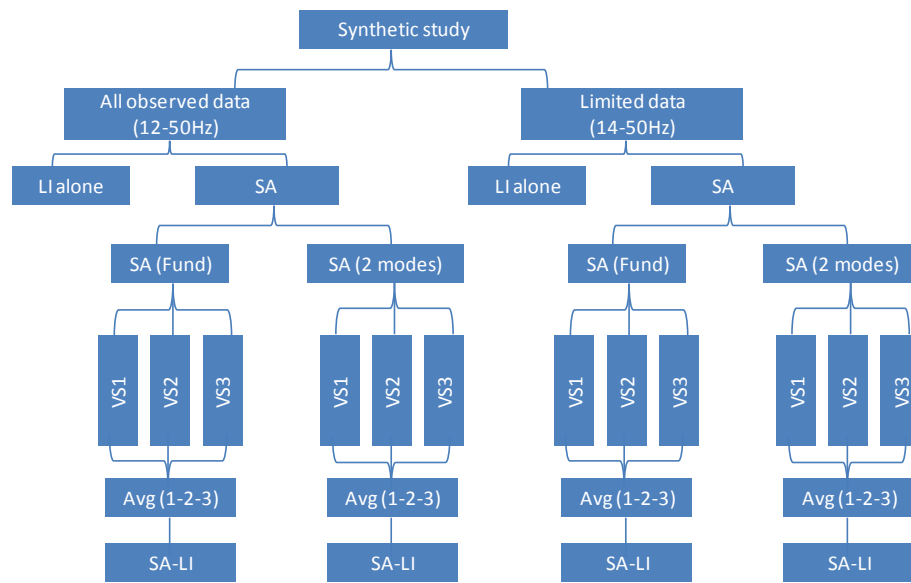Figure 5.1. Synthetic study: a) Target VS profile. b) Target DCs generated from SWAMI.

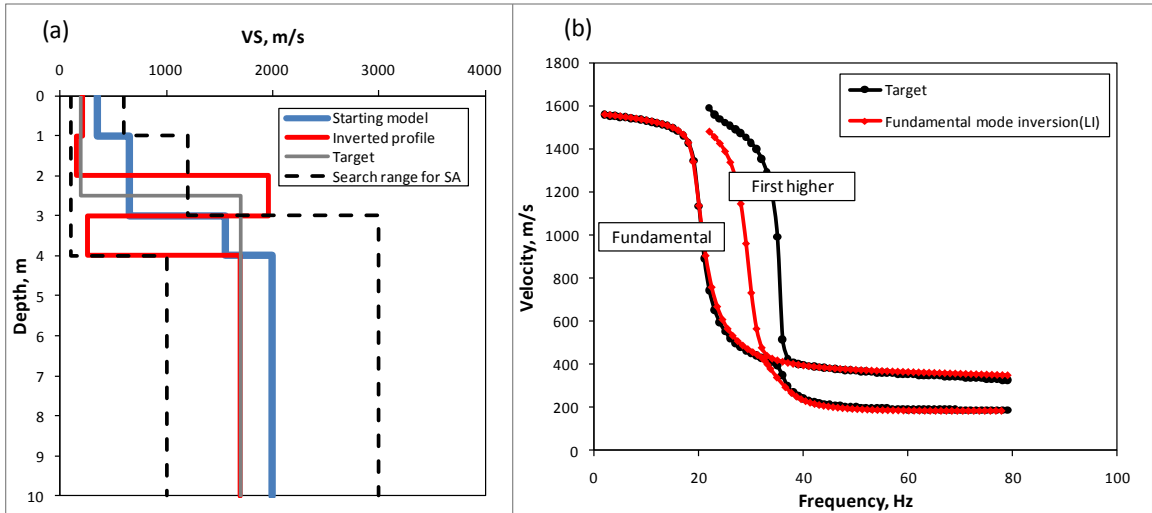Figure 5.2. Hierarchy of synthetic study with all observed data and limited data.

Figure 5.3 Synthetic study (all observed data), inversion with LI alone: a) VS profiles; b)
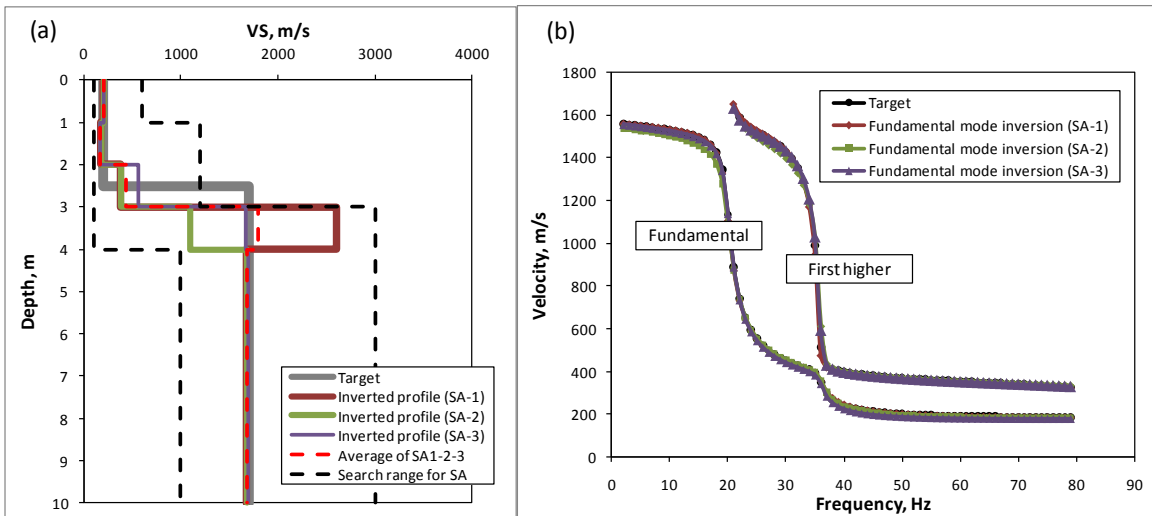
dispersion curves

Figure 5.4. Synthetic study (all observed data), inversion with SA (fundamental mode): a)
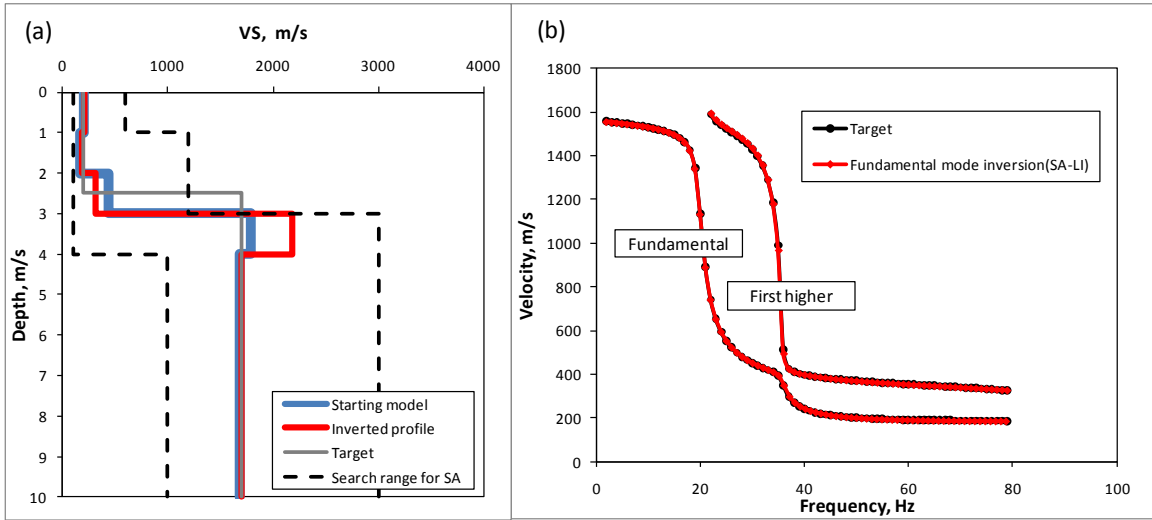
VS profiles; b) dispersion curves

59

Figure 5.5. Synthetic study (all observed data), inversion with SA (fundamental mode) -
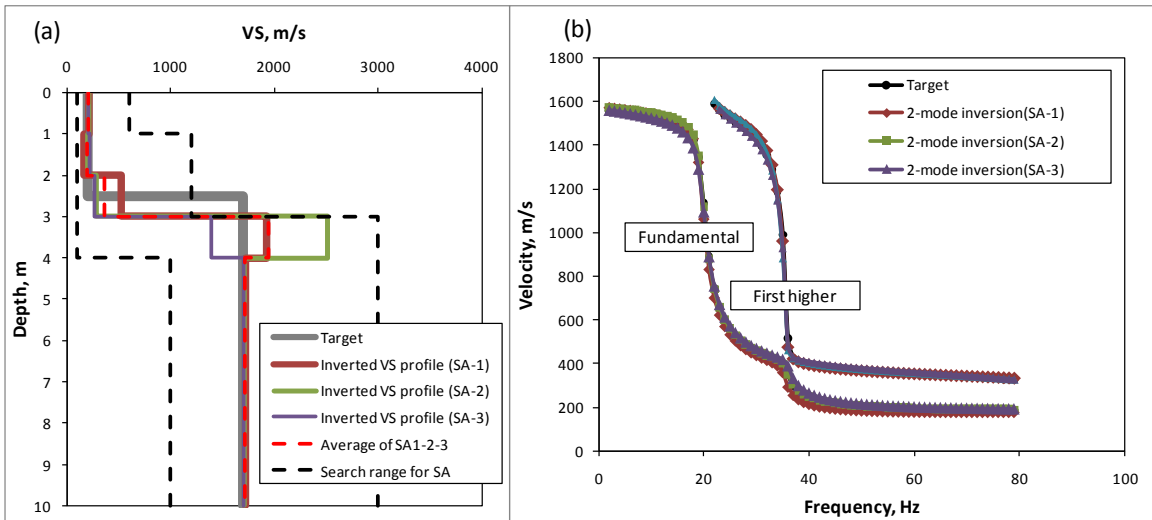
LI: a) VS profiles; b) Dispersion curves

Figure 5.6. Synthetic study (all observed data), inversion with SA (two modes): a) VS
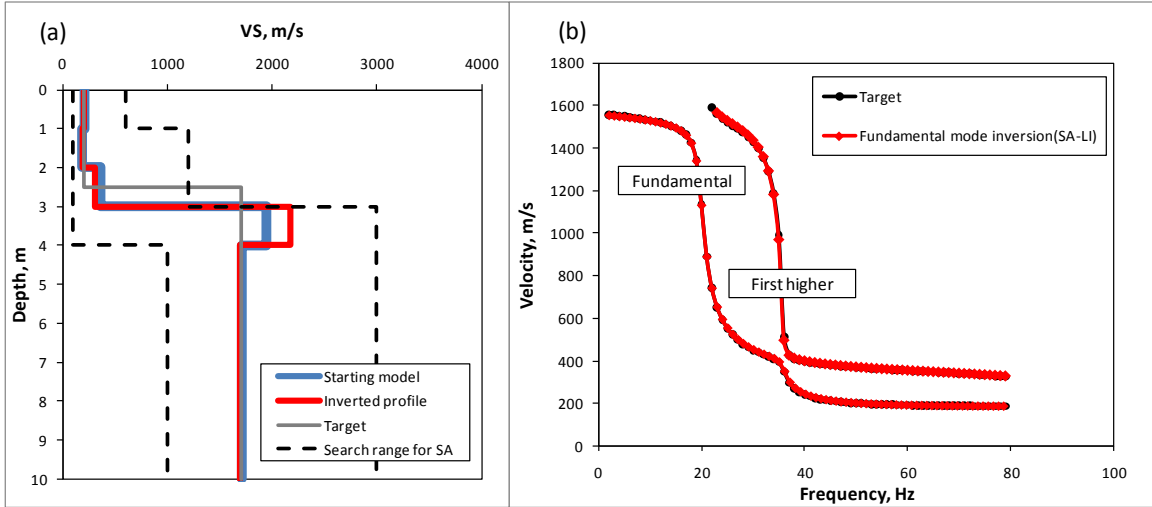
profiles; b) dispersion curves

60

Figure 5.7. Synthetic study (all observed data), inversion with SA (two modes) - LI: a)
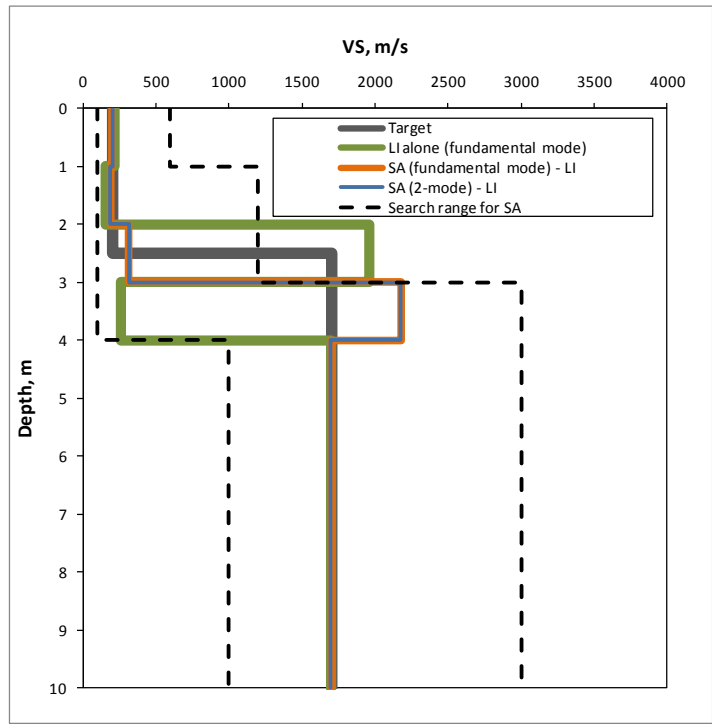
VS profiles; b) dispersion curves

Figure 5.8. Synthetic study (all observed data): VS profiles from fundamental mode

inversion with LI alone, fundamental mode inversion with SA-LI and two-mode

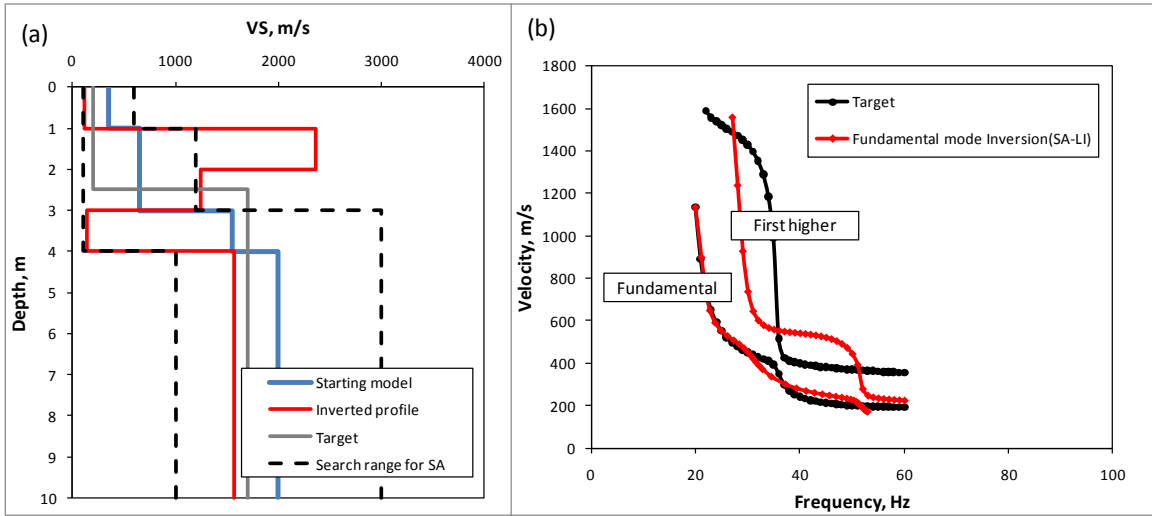inversion with SA followed by LI for fundamental mode.

61

Figure 5.9. Synthetic study (limited data), inversion with LI alone: a) VS profiles; b)
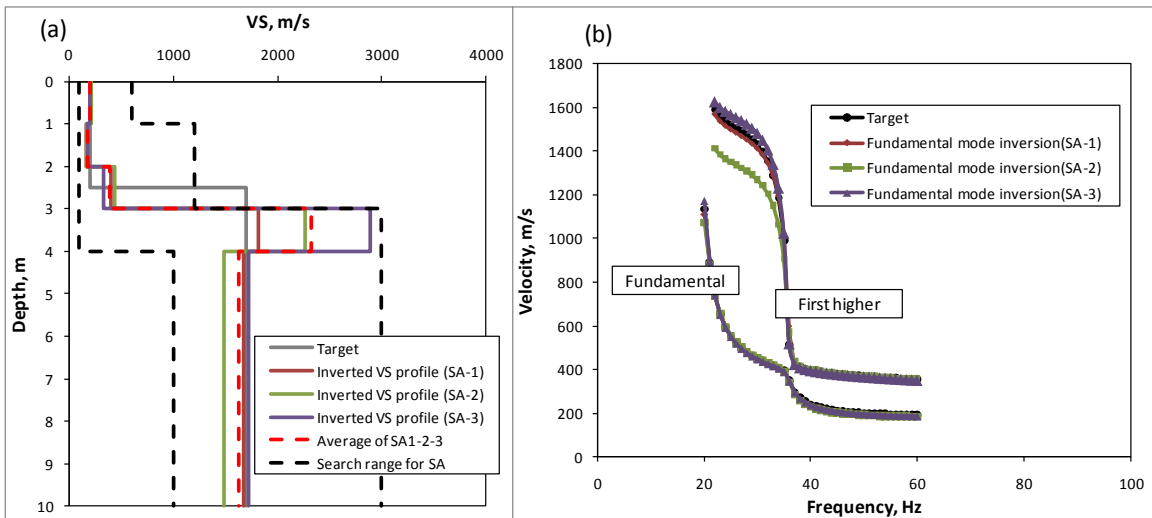
dispersion curves

Figure 5.10. Synthetic study (limited data), inversion with SA (fundamental mode): a) VS

profiles; b) dispersion curves

Figure 5.11. Synthetic study (limited data), inversion with SA (fundamental mode) - LI:

a) VS profiles; b) dispersion curves

Figure 5.12. Synthetic study (limited data), inversion with SA (two modes): a) VS

profiles; b) dispersion curves

63
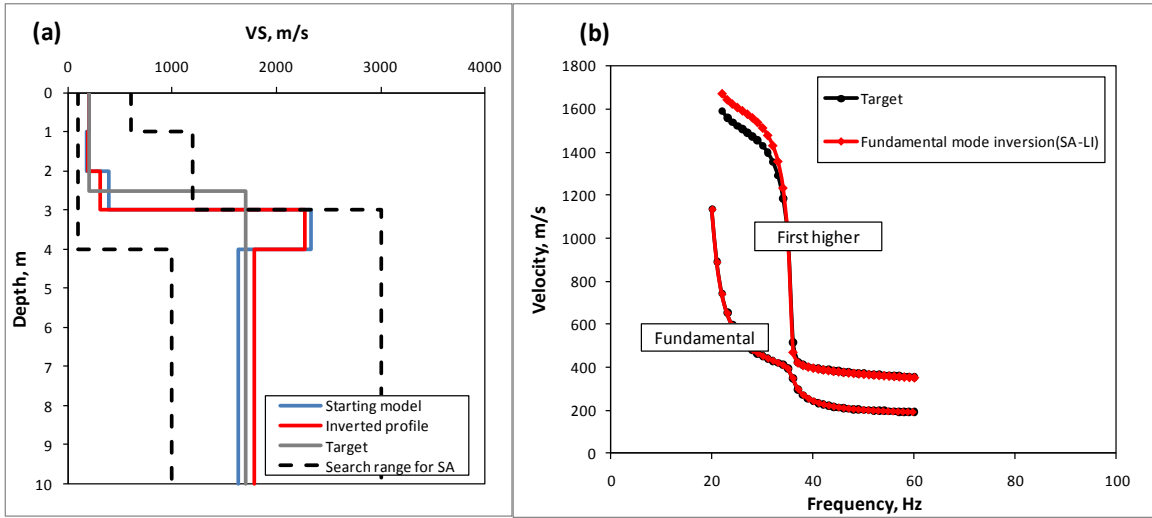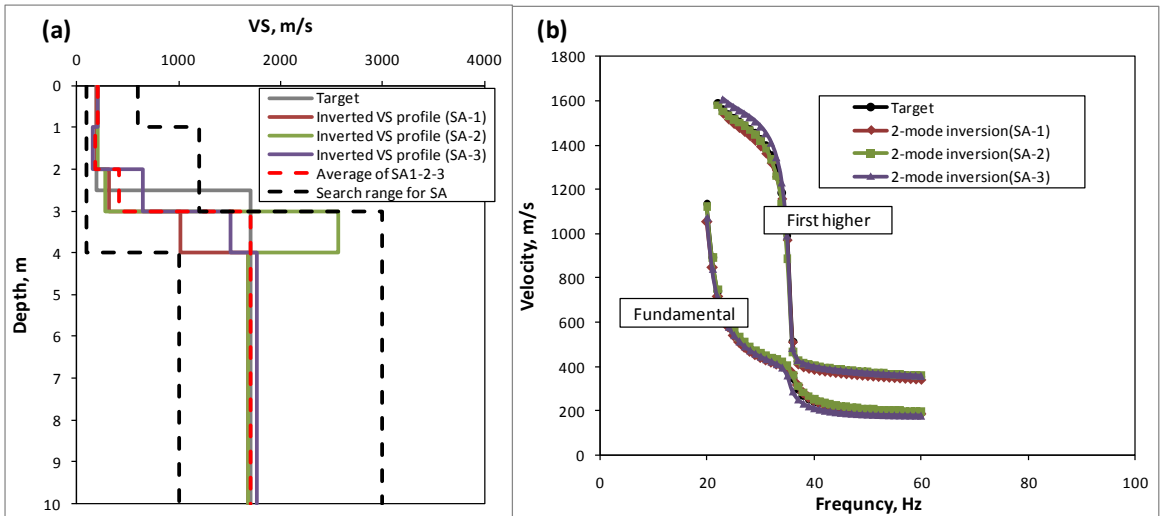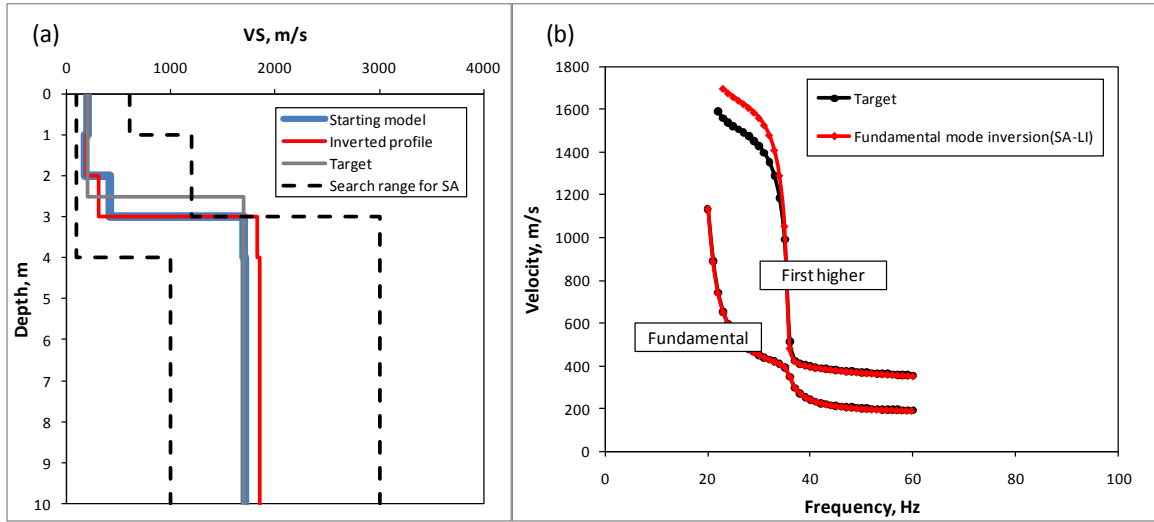
Figure 5.13. Synthetic study (limited data), inversion with SA (two modes) - LI: a) VS

profiles; b) dispersion curves
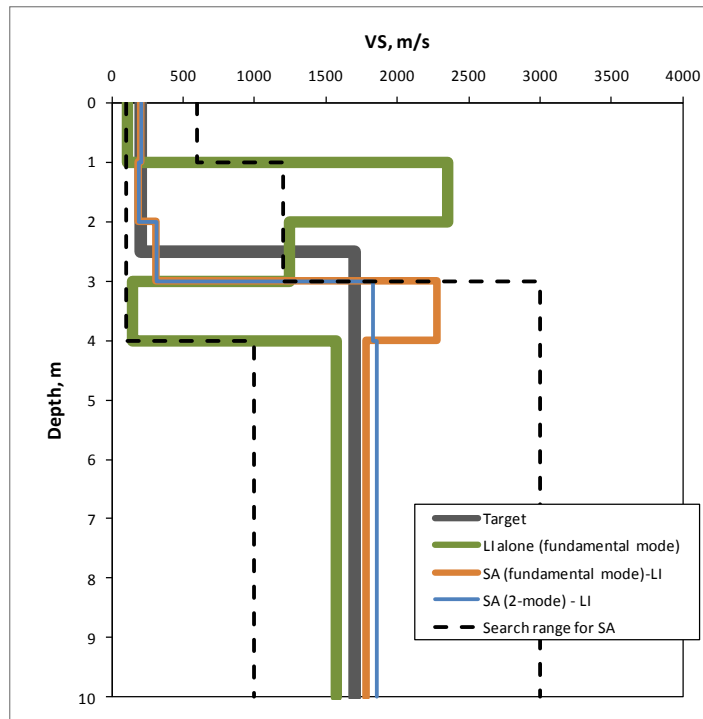
Figure 5.14. Synthetic study (limited data): VS profiles from fundamental mode inversion

with LI alone, fundamental mode inversion with SA-LI and two-mode inversion with SA

followed by LI for fundamental mode.
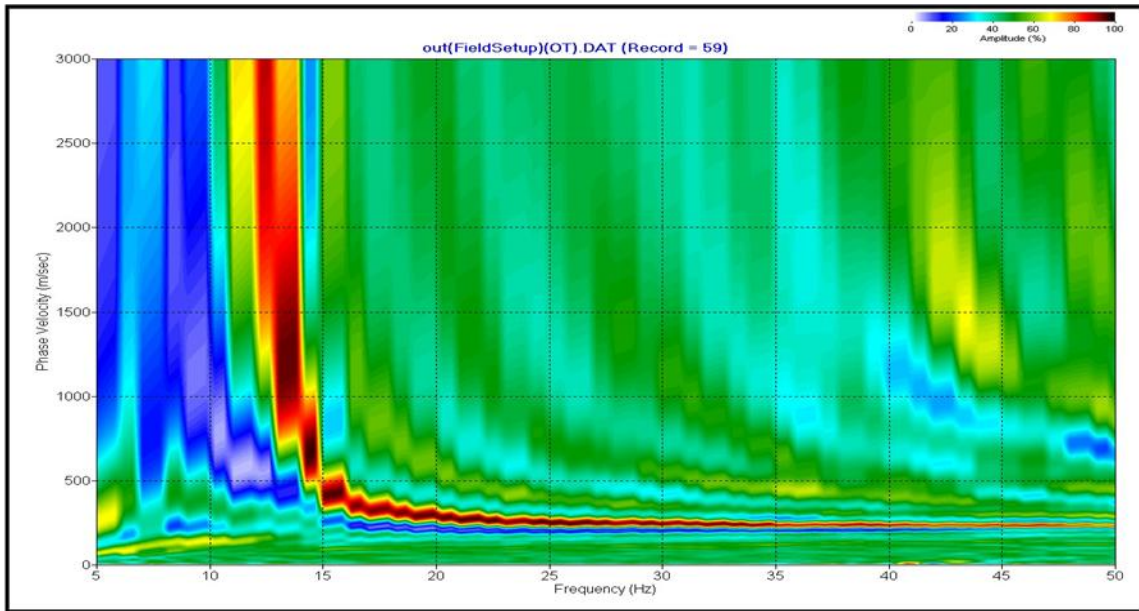
Figure 5.15. An overtone image of the surface-wave dataset created using Surfseis software. The dataset and the software used to create this image are the same used by Casto et al. (2009). The "normal" algorithm is assigned to obtain the overtone image. The resolution of the image is optimized to observe the higher modes.
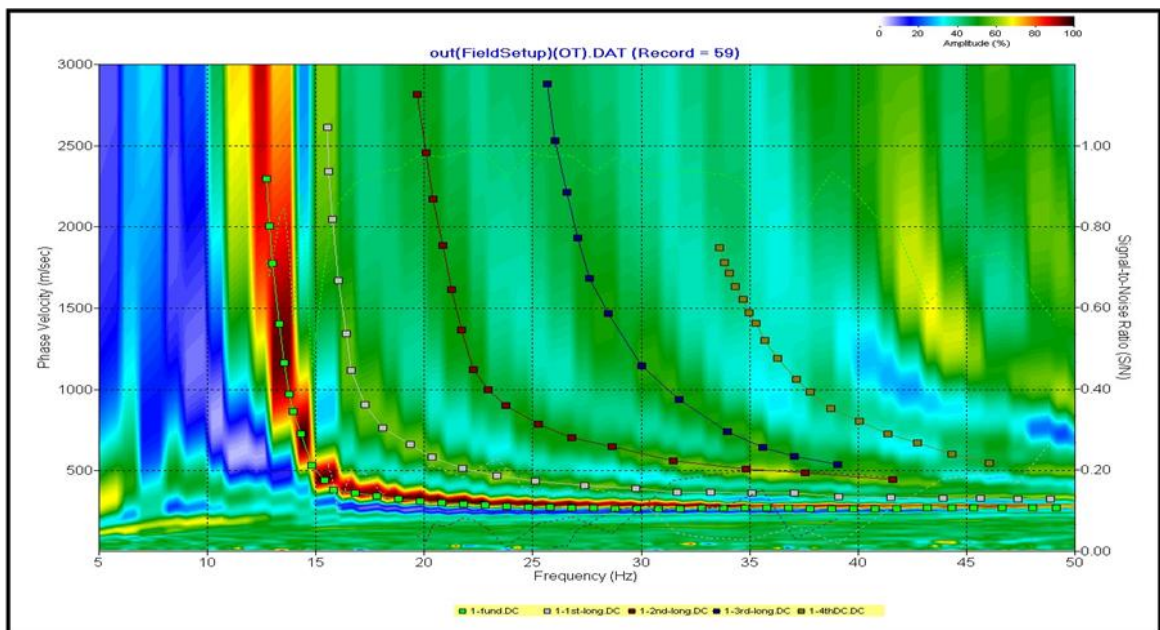
Figure 5.16. Fundamental mode and higher mode DCs picked from the overtone image shown in Figure 5.15.

65
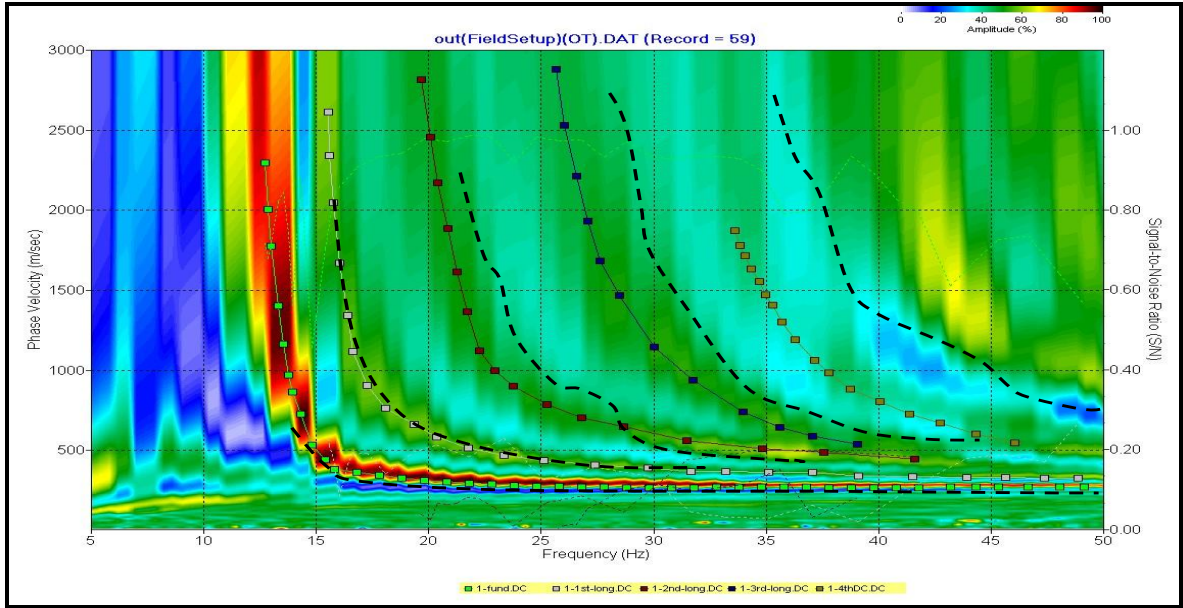
Figure 5.17. The black dashed lines represent multi-modal DCs of Casto et al. (2010) and are overprinted on Figure 5.16.
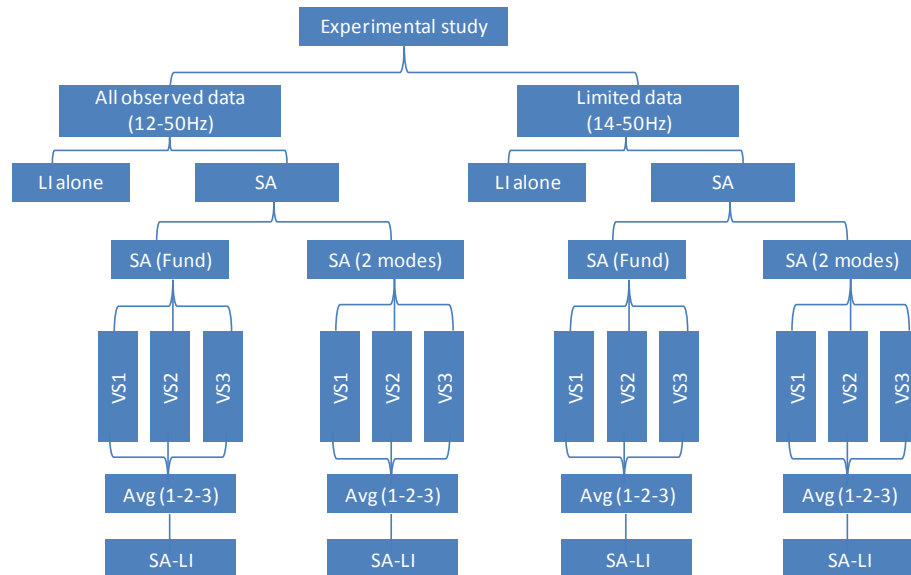
Figure 5.18. Hierarchy of experimental study with all observed data and reduced dataset.
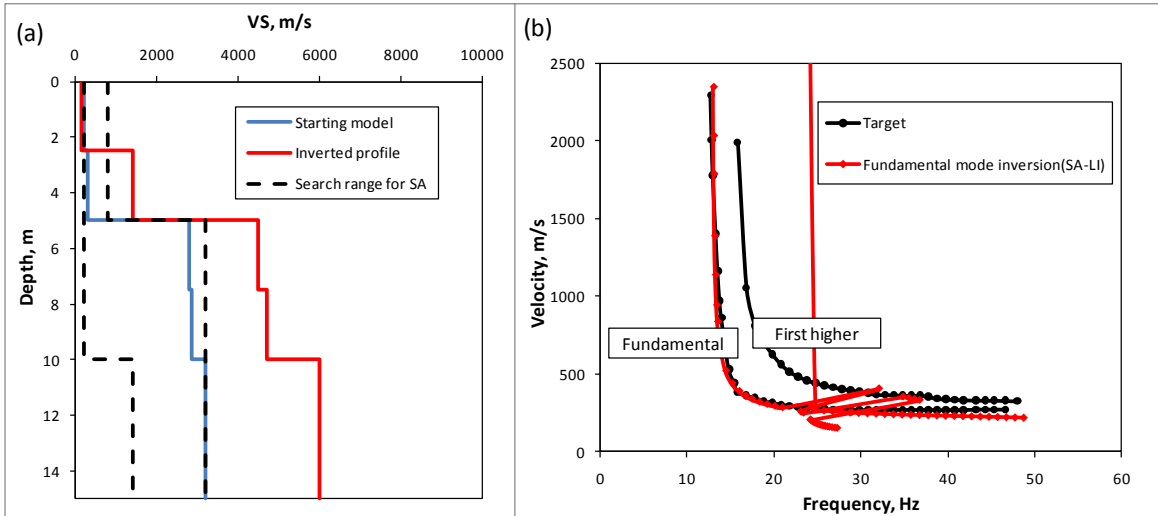
Figure 5.19. Experimental study (all observed data), inversion with SA (fundamental

mode) - LI: a) VS profiles b) dispersion curves
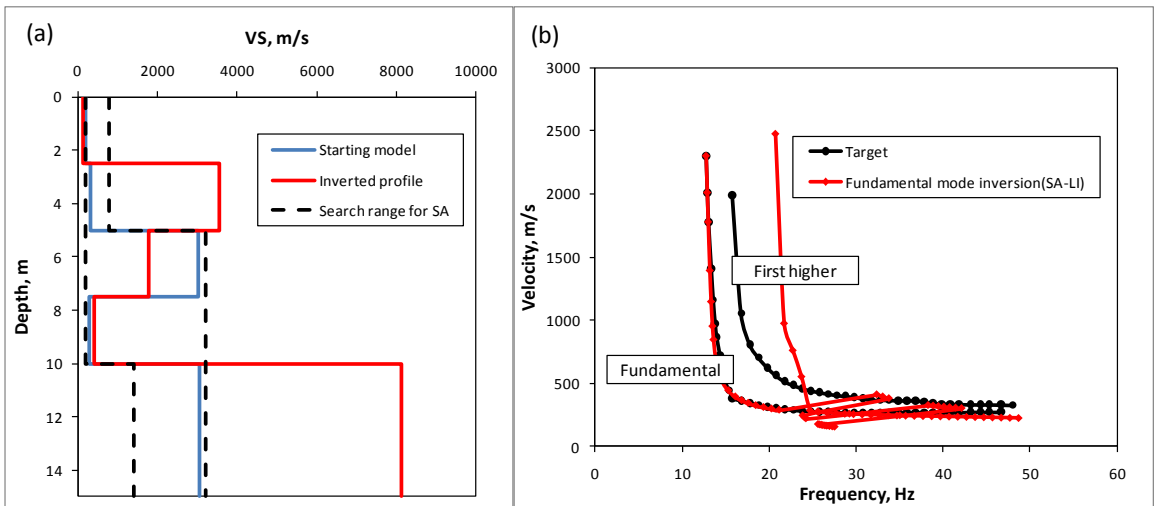
Figure 5.20. Experimental study (all observed data), inversion with SA (two modes) - LI:

a) VS profiles; b) dispersion curves
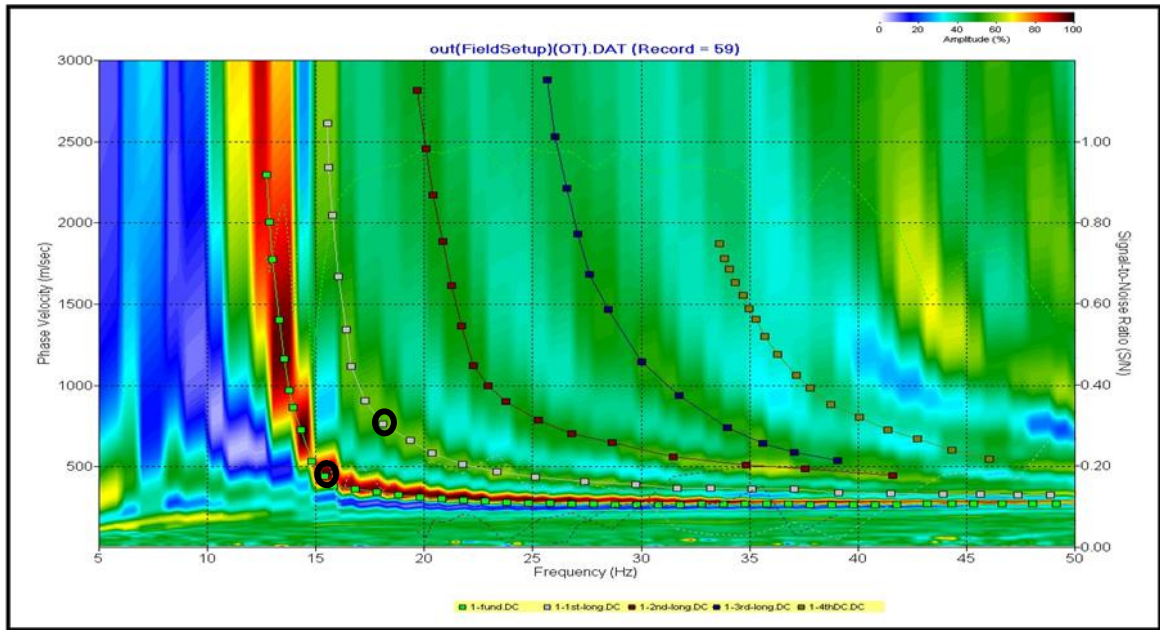
Figure 5.21. The dispersion data for frequencies below the black circled points are

disregarded for the experimental study.
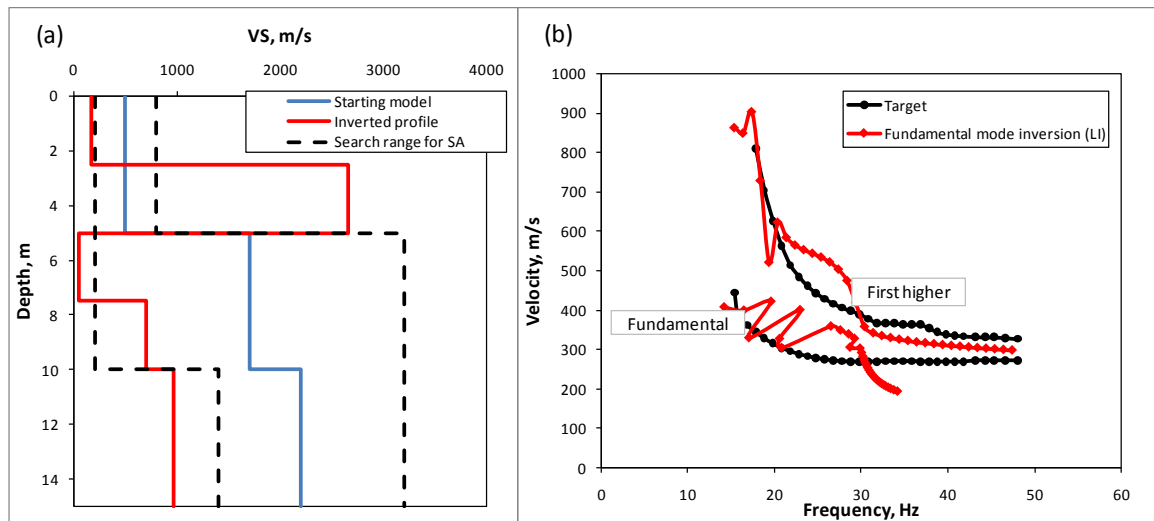
Figure 5.22. Experimental study (reduced dataset), inversion with LI alone; a) VS

profiles; b) dispersion curves

68
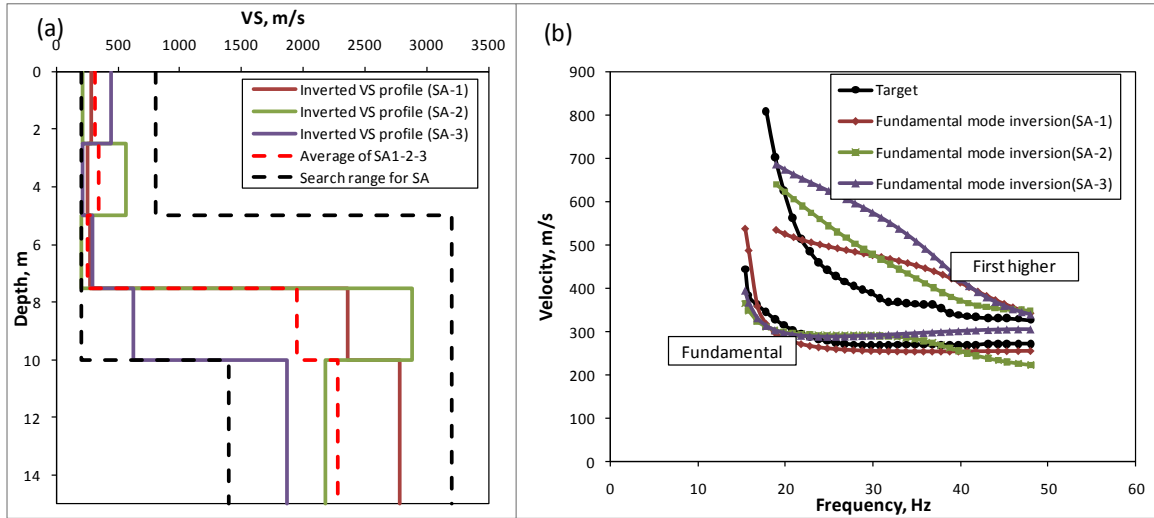
Figure 5.23. Experimental study (reduced dataset), inversion with SA (fundamental

mode): a) VS profiles b) dispersion curves
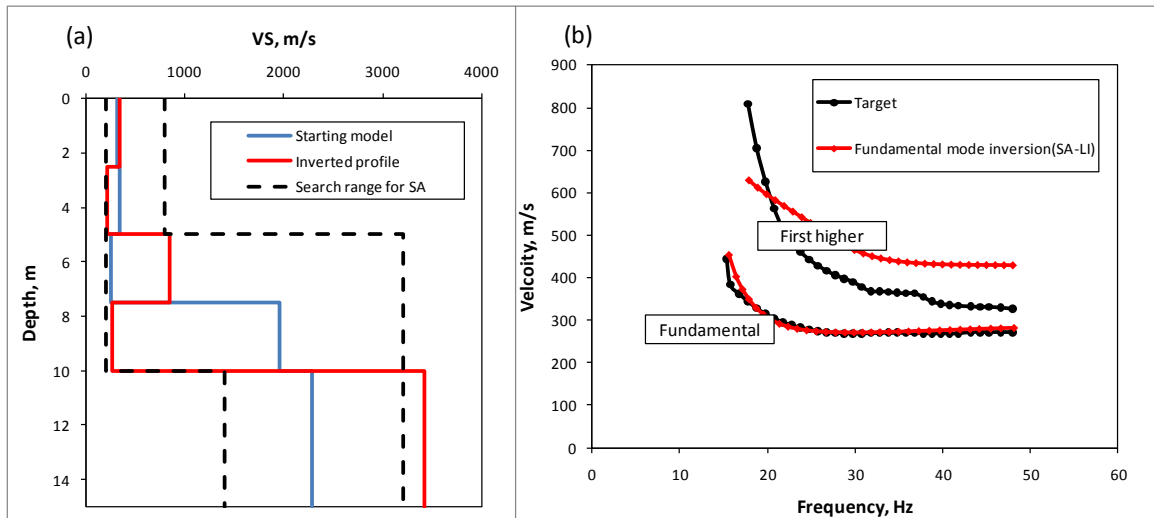
Figure 5.24. Experimental study (reduced dataset), inversion with SA (fundamental

mode) - LI: a) VS profiles b) dispersion curves

69
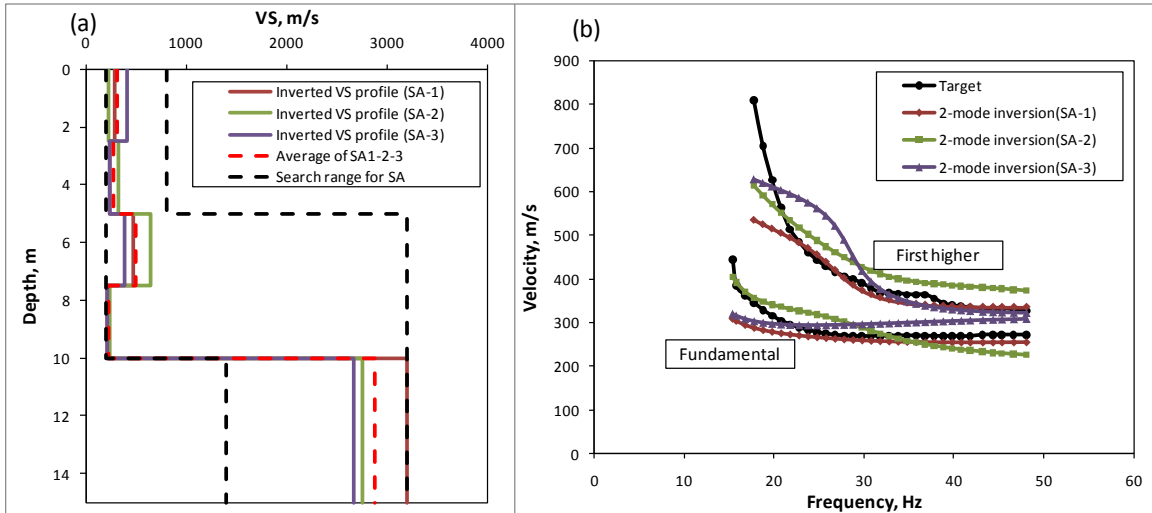
Figure 5.25. Experimental study (reduced dataset), inversion with SA (two modes): a) VS

profiles; b) dispersion curves
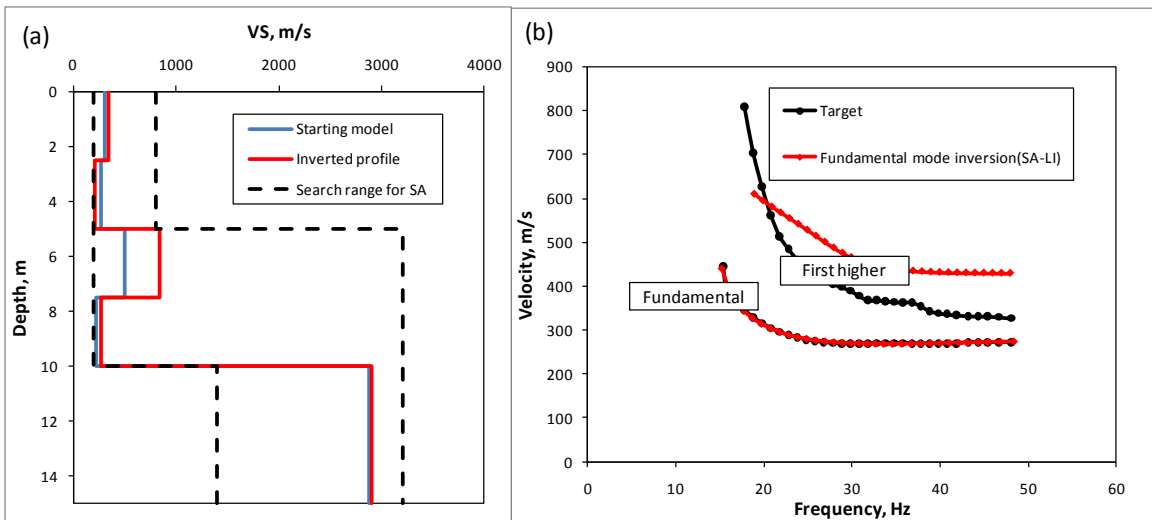
Figure 5.26. Experimental study (reduced dataset), inversion with SA (two modes) - LI:

a) VS profiles; b) dispersion curves

70
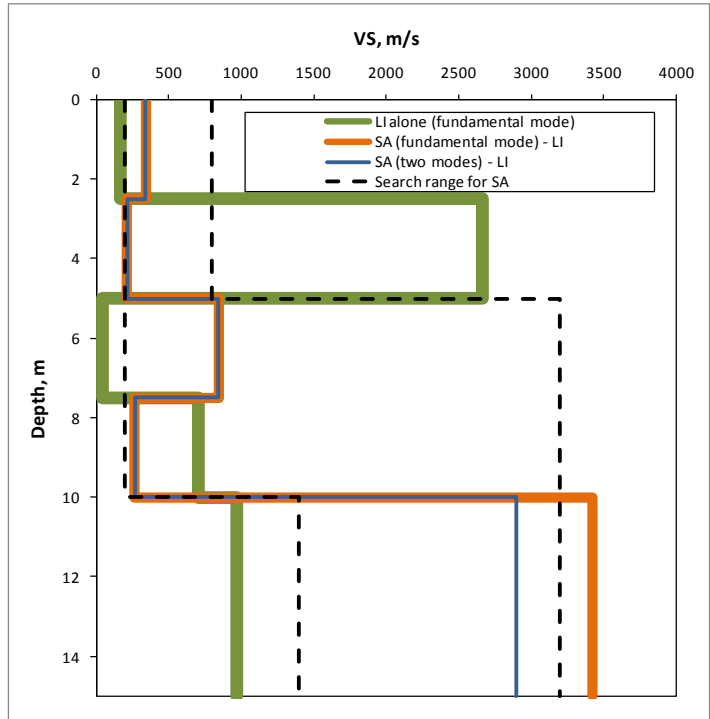
Figure 5.27. Experimental study (reduced dataset): VS profiles from fundamental mode inversion with LI, fundamental mode inversion with SA-LI and two-mode inversion with SA followed by LI for fundamental mode.

CHAPTER 6

POTENTIAL FOR MISINTERPRETATION OF MULTI-MODAL DATA

6.1 Introduction

As discussed in Chapter 1, the Rayleigh wave energy is partitioned to higher modes in the presence of a high impedance contrast boundary (HICB). Useful estimates of VS profiles for shallowly buried bedrock using seismic surface waves might require higher modes; this was demonstrated in Chapter 3. But the higher mode dispersion curves (DC) can be difficult to identify in the overtone image (e.g., Gabriels et al., 1987; Strobbia and Foti, 2006; Calderón-Macías and Luke, 2010).

In this chapter, the consequences were studied for the misinterpretation of a part of the first higher mode DC to be the fundamental mode DC in a high velocity halfspace (HVH) profile.

6.2 Misinterpretation of DCs of an HVH profile

Calderón-Macías and Luke (2010) observed the possibility of misinterpreting part of the first higher mode DC as the fundamental mode DC for the HVH model. The relevant mechanical properties of the HVH model studied by the authors are shown in Table 6.1. The authors modeled a field test condition with a vertical source and surface-mounted receivers on an HVH profile by using the finite difference method. An overtone image was developed for the HVH model from the finite difference computations. The authors also computed multi-modal DCs for the same HVH model from the forward modeling algorithm SWAMI (Rix and Lai, 2005). The synthetically computed DCs were imprinted over the velocity-frequency map. The authors found that the first higher mode DC appeared to intersect with the fundamental mode DC, and that the resolution of the

72

velocity-frequency map was poor for both modes at the low frequencies. Together, these two characteristics indicated possibility for misinterpretation of the DCs. On the other hand, Jin et al. (2009) conducted synthetic studies on a VS model having a high velocity layer at shallow depth and illustrated that DCs could be misinterpreted even when the resolution of the overtone image is good at fairly low frequencies.

6.3 Kink in a dispersion curve

One of the major causes of misinterpretation is due to the formation of a "kink" in a DC. A kink is a sudden bulge-out portion in a DC toward the direction of the velocity axis in the plot of velocity versus frequency. Calderón-Macías and Luke (2010) showed a kink appearing in the fundamental mode DC for a profile that has an HICB. When Jin et al. (2009) studied a theoretical VS profile with a high velocity layer at shallow depth, i.e., a profile with two HICBs, they found a kink in the fundamental mode DC. The DCs of the fundamental mode and first higher mode appeared to nearly intersect in the vicinity of the kink. Bergamo et al. (2011) also saw that the theoretical DCs of the fundamental mode and the first higher mode developed to fit the experimental DCs tended to intersect at high frequencies in their analyses of analyzed surface-wave data for thin fill sediment over limestone bedrock. We conclude that the tendency of the curves to intersect can be related to formation of a kink in the fundamental mode DC.

A theoretical HVH model, the same as the base model introduced in Chapter 2, is selected in order to study the formation of a kink. DCs were computed for models having velocities of halfspace ranging from 200 m/s, that is, no contrast, to 1700 m/s in six steps at intervals of 300 m/s. These DCs are shown in Figure 6.1, which illustrates the occurrence of kinks in the fundamental mode DCs. The kink appears when the VS of the

73

halfspace is at 800 m/s; and becomes more pronounced above 800 m/s. The kink is seen only in the fundamental mode DC and not in the first higher mode DC.

The trend of the maximum amplitude spectra of phase velocity in an overtone image guides the user to identify a DC. In the work of Calderón-Macías and Luke (2010), the maximum amplitude spectra of phase velocity became obscure at frequencies below the location of the kink. In such a situation, we propose that the user can be distracted from selecting the actual fundamental mode DC around the location of the kink, and may erroneously incorporate the low-frequency portion of first higher mode DC as part of the fundamental mode DC. This erroneous DC which consists of parts of the fundamental mode and the first higher mode is named as a misinterpreted DC.

6.4 Inversion

Figure 6.2 shows the DCs of the fundamental mode and first higher mode for the profile described in Table 6.1; these DCs are computed with the forward modeling algorithm SWAMI (Rix and Lai, 2005). The misinterpreted DC is marked as a red dashed line and assumed as the fundamental mode DC. In order to obtain a VS profile, the linearized inversion method presented in Chapter 5 was applied to the misinterpreted and the correct fundamental-mode DCs, separately. Both inversions were performed using the same starting model. The parameters of the starting model are shown in Table 6.2. The density was held constant at 1700 and 2200 kg/m^3 for the layers and halfspace, respectively. Similarly, the Poisson's ratio was also held constant for the layers and halfspace at 0.3 and 0.25, respectively. As the original HVH profile (Table 6.1) consists of a 10-m thick layer above the halfspace, the depth to halfspace was also maintained as 10 m in the starting model. In other words, we assumed that independent information about the depth to halfspace was available from sources such as drill log or seismic

74

refraction data. The layer above the halfspace was divided into five sub-layers of equal thickness, and the velocity of the sediment in the starting model increased gradually with depth.

The inverted VS profiles for the correct and misinterpreted DCs are tabulated in Table 6.2. Figure 6.3 and Figure 6.4 show curve fits for the correct and misinterpreted DCs, respectively. The theoretical DC perfectly fits the correct DC, as expected. The misinterpreted DC also shows a good fit with its target DC except at frequencies below 13 Hz. The inverted VS profiles for both DCs are shown in Figure 6.5. The inverted VS profile for the correct DC is very close to the actual profile. But, for the misinterpreted DC, a high velocity layer at the depth 4 m appears. Low velocity layers are formed below and above this high velocity layer. The inverted VS of the halfspace is 41 % higher than the expected velocity.

6.5 Effect of misinterpretation

The misinterpretation of fundamental mode DC for the shallow bedrock site may result in significant, unrealistic velocity fluctuations including a suspiciously high velocity layer at a shallow depth and excessively high VS of halfspace. As a result, the average velocity of the profile would be overestimated. As noted by Pitilakis et al. (2004), such overestimation could affect site classification. This type of erroneous result might be tested in the field by borehole log or seismic refraction data. However, in the particular case where an HVH truly exists, as in arid areas such as Las Vegas, Nevada, where a stiff layer of sediments formed by the calcite cementation of sand and gravel is commonly found in the subsurface (Werle and Luke, 2007), a VS profile with strong contrasts might be realistic.

75

Table 6.1. Model properties of an HVH profile studied by Calderón-Macías and Luke (2010).

Layer	VS (m/s)	Thickness (m)	Poisson's ratio	Density (kg/m^3)
L1	300	10	0.30	1700
Halfspace	1500	N/A	0.25	2200

Table 6.2. Model properties for the starting model, and inverted profiles for the correct and misinterpreted DCs.

Layer	Thickness (m)	Poisson's ratio	Density (kg/m^3)	Velocity (m/s) from		
				Starting model	Correct DC	Misinterpreted DC
L1	2	0.3	1700	200	291	430
L2	2	0.3	1700	400	313	168
L3	2	0.3	1700	600	284	1259
L4	2	0.3	1700	800	326	183
L5	2	0.3	1700	1000	285	1251
HS	--	0.25	2200	1200	1467	2089
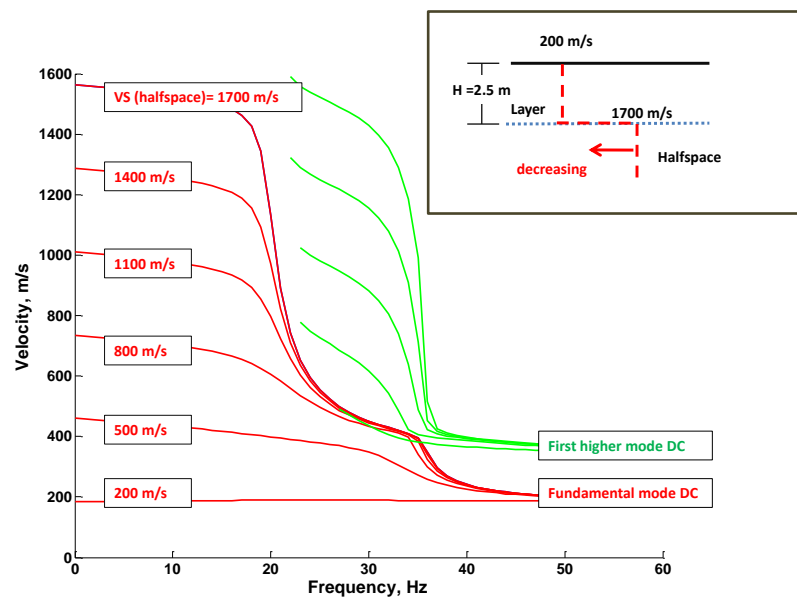
Figure 6.1. Appearance of kinks in the fundamental mode DCs due to presence of an HICB. The lowermost DC of the first higher mode (green) is for halfspace velocity of 500 m/s. The first higher mode DC does not appear when the layer velocity and halfspace velocity are both assigned as 200 m/s.

76
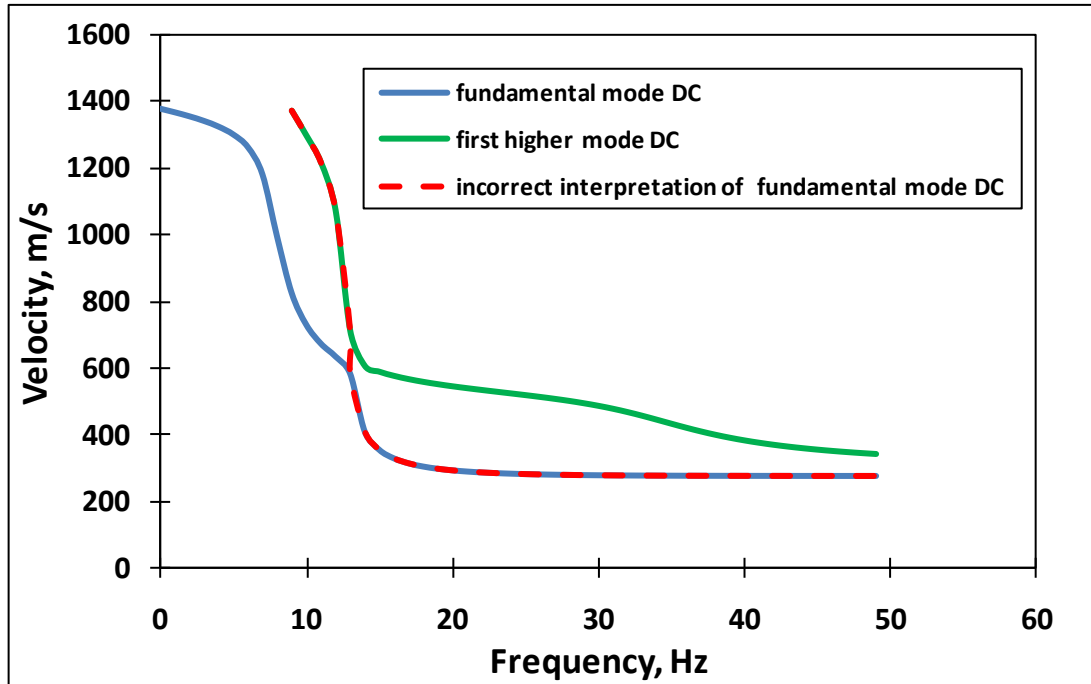
Figure 6.2. Synthetically computed DCs (solid lines) for the model parameters listed in Table 6.1. The misinterpreted DC (red dashed line) formed from a combination of the DCs of the fundamental mode and first higher modes.
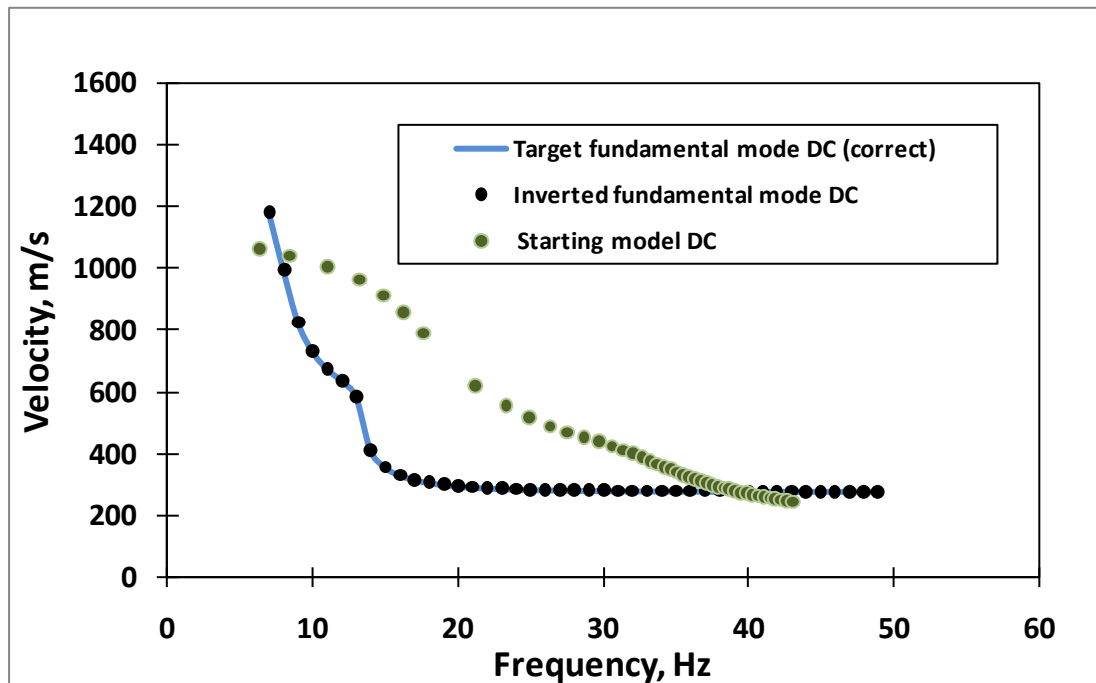
Figure 6.3. Inversion of the correct fundamental mode DC.

77

Figure 6.4. Inversion of the misinterpreted fundamental mode DC.

Figure 6.5. Shear-wave velocity profiles.

CHAPTER 7

DISCUSSION, CONCLUSIONS AND RECOMMENDATIONS

7.1 Discussion

Inversion of surface-wave data is a non-linear inverse problem, and can lead to a non-unique solution. A high velocity halfspace (HVH) representing shallow bedrock presents a high impedance contrast boundary (HICB) that is responsible for partitioning of Rayleigh wave energy to higher modes. Rayleigh-type surface wave data that are collected using a sledgehammer or an accelerated weight drop a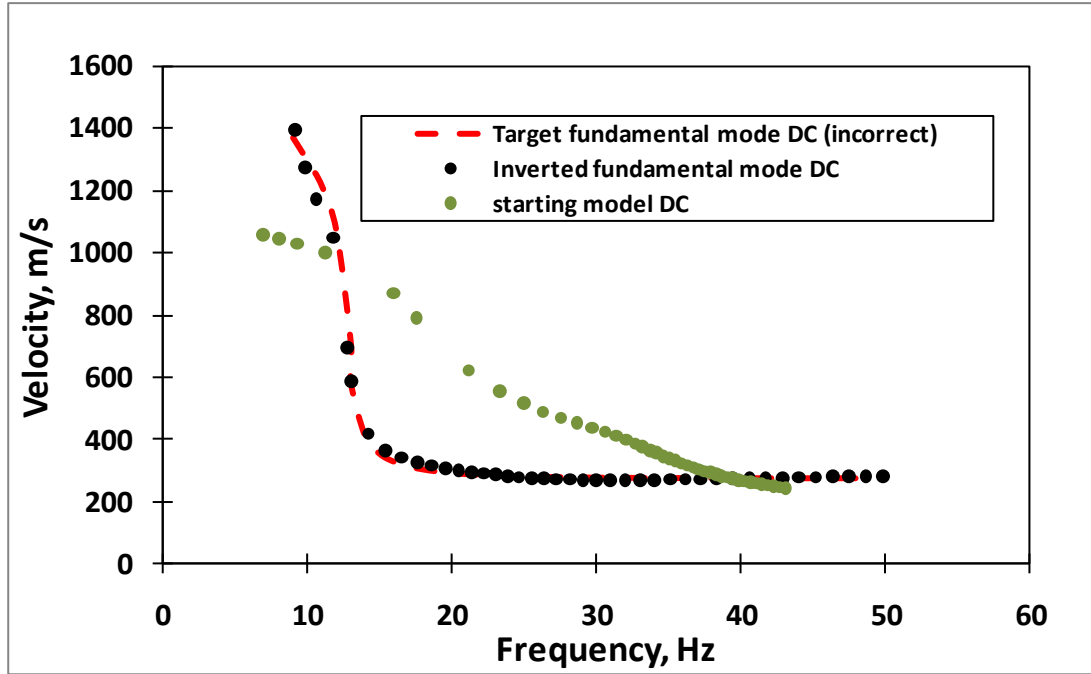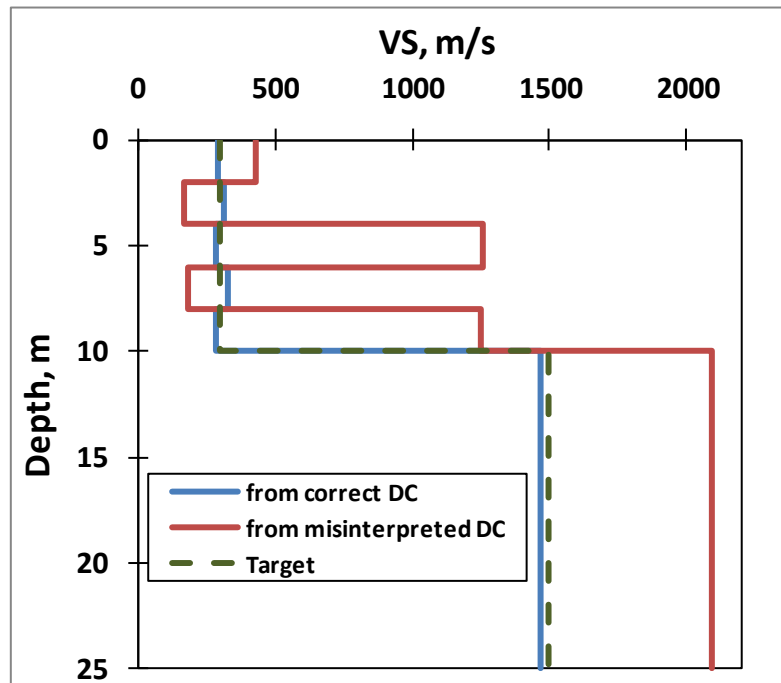s a source lack resolution in sufficiently low frequencies to characterize bedrock well by fundamental mode alone, even if it occurs at very shallow depth.

To further complicate the problem, dispersion curves (DCs) can be difficult to pick from an overtone image. Because of energy partitioning and reduced resolution at low frequencies, a user might misinterpret a portion of the first higher mode at low frequencies to be a part of the fundamental mode DC. For a particular HICB case studied, inversion of the DC misinterpreted in this way resulted in an erroneously high velocity layer in the shear-wave velocity (VS) profile with too-high estimation of the VS of the halfspace, yielding average VS that is overall too high.

The low frequency component of a fundamental-mode DC represents the bedrock component of the profile. Even if mode misidentification were not a concern, for practical reasons, the fundamental-mode DC may lack low frequencies in the sampling window (the frequency band observed in practice), thereby providing inadequate information to resolve VS of the bedrock. On the other hand, portions of the higher-mode DCs are sometimes observed within the sampling window. Within the sampling window, these DCs are more sensitive to changes in the VS of bedrock than is the fundamental

79

mode DC. So, in theory, the higher mode DCs can provide information regarding the VS of bedrock that is missing from the portion of the fundamental mode DC that appears in the sampling window.

Parametric studies of root-mean-square error surfaces for a simple HICB profile showed that in limiting the dataset to a likely sampling window, the ability of the inversion process to resolve VS of the halfspace is reduced. For the case studied, simultaneous consideration of the fundamental mode and first higher mode would significantly improve ability to resolve depth and slightly improve ability to resolve velocity of the halfspace. The studies highlighted the importance of correct layer geometry in the starting model in the typical inversion process which does not optimize layer geometry.

Inversion tests of the same simple HICB profile demonstrated that when a full range of frequencies was included in the target DC, a reasonable solution resulted when fundamental mode alone was considered, and consideration of a higher mode did not improve results. When the dispersion curve was limited to a narrow frequency band, results improved when a higher mode was considered jointly with the fundamental mode. Of all tests run, this last test (using a limited frequency band with a well-informed starting model that considers two modes) recovered the best match to the target VS profile.

Inversion tests of experimental data taken at an HICB site demonstrated the possibility of misinterpretation of the DCs at low frequencies. When inversion was conducted using a subset of the picked DC that was expected to be free of contamination due to mis-picks, credible VS models were recovered from both SA tests, considering fundamental mode alone and considering two modes. The tests did not demonstrate

conclusively that the incorporation of higher modes in inversion improved ability to estimate a reasonable VS profile, however, the tests did show that improving the data fit to just the fundamental mode DC (by way of applying LI to the results of SA) degraded the quality of the VS profile.

Both the experimental and synthetic studies confirmed prior research indicating that a well-informed starting model is required to obtain a credible solution in inversion of surface-wave data collected at a site with a HICB.

Synthetic studies demonstrated that investigation of the shape of the DC to find the point of maximum curvature at long wavelength can be helpful to estimate the depth to halfspace in order to refine the starting model.

7.2 Conclusions

A suite of tests was conducted to address the topic of estimating the depth and VS of shallow bedrock by utilizing multi-modal surface-wave data in a frequency band limited by practical considerations. Picking of the experimental dispersion curve can be complicated by the tendency of the modes to overlap at low frequencies. Testing demonstrated that impacts of such mis-picks are manifested in extreme fluctuations in the VS profile and too-high VS of the halfspace. In theory, the higher mode DCs can provide information regarding the VS of bedrock that is missing from that portion of the fundamental mode DC that can be resolved in practice.

Multiple analyses of simple profiles representing shallow bedrock demonstrated that a well-informed starting model for inversion is necessary to obtain a credible solution. Layer geometry deserves careful consideration. An algorithm that can be used to improve the starting model by estimating the depth to the high impedance contrast boundary through observation of the experimental dispersion curve is presented and tested.

81

In idealized tests, use of the full dispersion dataset was able to recover the target VS profile with fundamental-mode data alone, while similar tests using a frequency-limited dataset were not. In the latter case, results of inversion improved when a higher mode was considered jointly with the fundamental mode. Outcomes of similar tests on experimental data from a shallow bedrock site were less definitive.

7.3 Recommendations

Recommendations for future research, based on the work presented here, are as follows.

Chapter 2: The upper bends of the fundamental-mode experimental DC could be studied more carefully for use in developing a high quality starting model. The lower bends or upper bends or a combination of both might be studied more rigorously to derive the relation for the VS of the layer and bedrock. The algorithm presented here might be extended to address a high velocity layer, i.e., a profile with two HICBs.

Chapter 3: Results from the analysis of surface-wave data for a shallow bedrock site depend primarily upon the following model parameters: 1) the VS of the overburden and bedrock and 2) the depth to bedrock. The anticipated site conditions can be used to design the surface-wave data collection. The plan would address a) the necessary frequency range of data collection and b) the field test configuration to include i) type and location of source and ii) type, spacing and configuration of sensors.

Chapter 4: RMS error surfaces can be used to study hypothetical VS profiles having multiple layers. A multi-dimensional set of error surfaces would be required to understand the importance and interrelationships of the many different model parameters involved in the inversion process. Their usefulness to establish parameter sensitivity in inversion of experimental datasets can be explored.

82

Chapter 5: Research presented in this chapter can be extended by: revising the dispersion curve picks for inversion, to explore further the extent to which the bedrock characteristics are captured in the higher mode; extend the inversion studies to use a linearized inversion algorithm that can solve for multiple modes; test SA results using a statistically significant number of iterations; consider three or more modes in inversion.

Chapter 6: Sensitivity studies using synthetic datasets might reveal patterns to help the user to identify and avoid the problem of mode misinterpretation in the presence of an HICB.

APPENDIX A: PICKING THE LOWER BENDS FROM DISPERSION CURVES OF

SYNTHETIC DATA

Figure A.1.A set of DCs obtained when the depth to bedrock changes from 2 m to 10 m in the increments of 2 m; the VSs of the layer and bedrock are held constant at 200 m/s and 1700 m/s, respectively. The dots shows in the plots are the wavelengths at which the lower bends occur.

Figure A.2. A set of DCs obtained when the depth to bedrock changes from 2 m to 10 m in the increments of 2 m; the VSs of the layer and bedrock are held constant at 200 m/s and 2300 m/s, respectively.
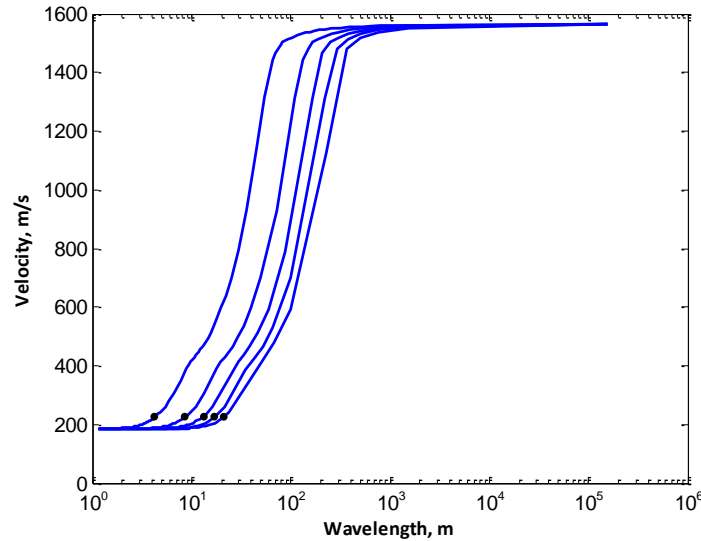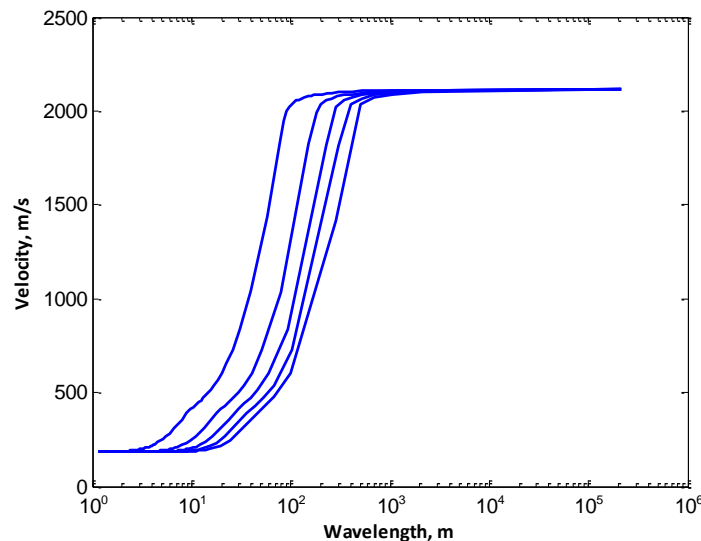
84

Figure A.3. A set of DCs obtained when the depth to bedrock changes from 2 m to 10 m in the increments of 2 m; the VSs of the layer and bedrock are held constant at 200 m/s and 2900 m/s, respectively.

Figure A.4. A set of DCs obtained when the depth to bedrock changes from 2 m to 10 m in the increments of 2 m; the VSs of the layer and bedrock are held constant at 500 m/s and 1700 m/s, respectively.

85

Figure A.5. A set of DCs obtained when the depth to bedrock changes from 2 m to 10 m in the increments of 2 m; the VSs of the layer and bedrock are held constant at 500 m/s and 2300 m/s, respectively.
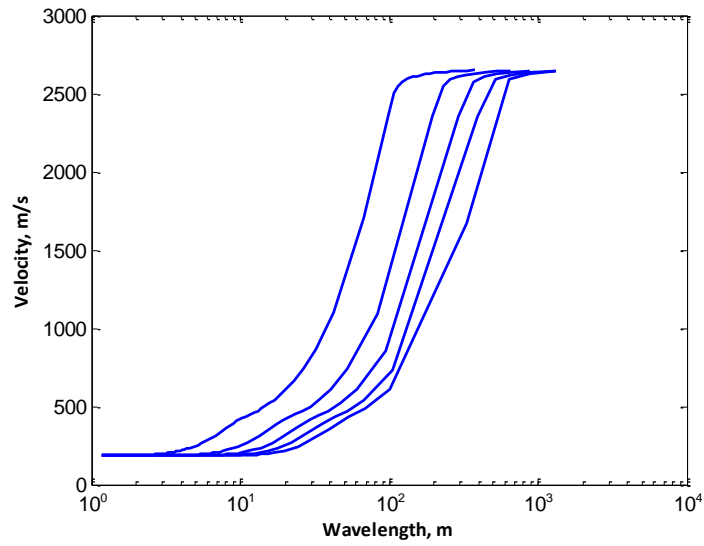

Figure A.6. A set of DCs obtained when the depth to bedrock changes from 2 m to 10 m in the increments of 2 m; the VSs of the layer and bedrock are held constant at 500 m/s and 2900 m/s, respectively.
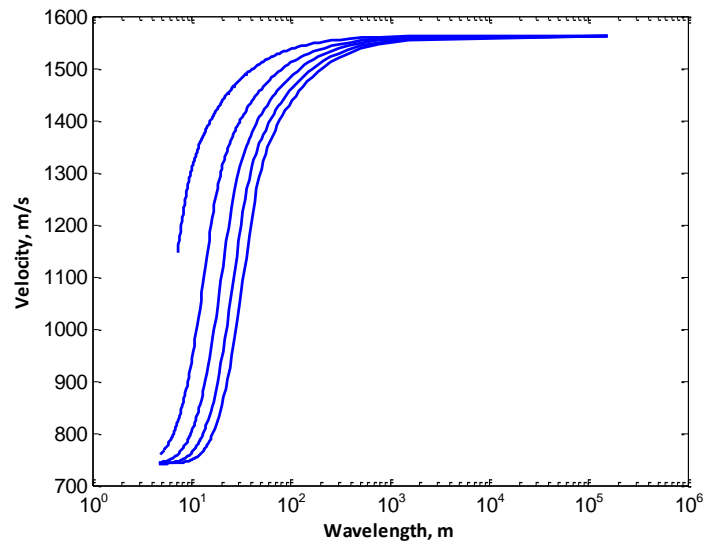
Figure A.7. A set of DCs obtained when the depth to bedrock changes from 2 m to 10 m in the increments of 2 m; the VSs of the layer and bedrock are held constant at 800 m/s and 1700 m/s, respectively.
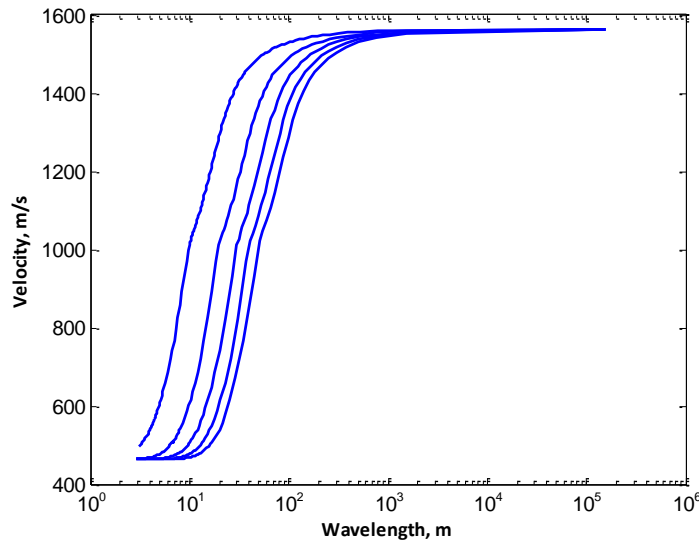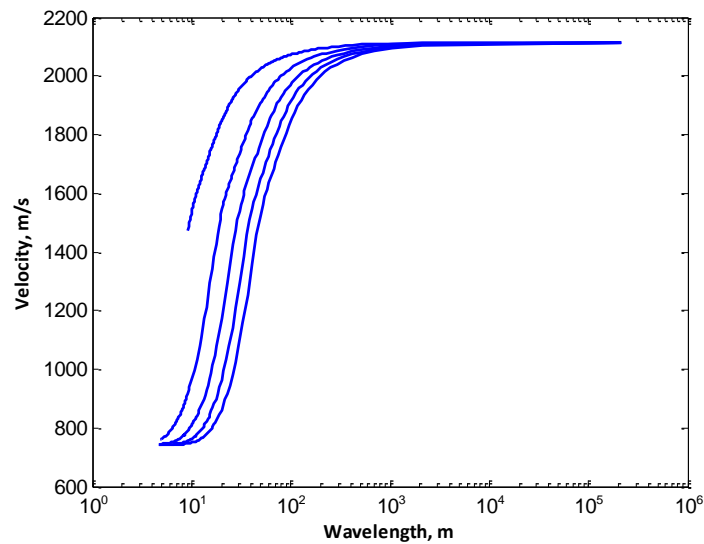

Figure A.8. A set of DCs obtained when the depth to bedrock changes from 2 m to 10 m in the increments of 2 m; the VSs of the layer and bedrock are held constant at 800 m/s and 2300 m/s, respectively.
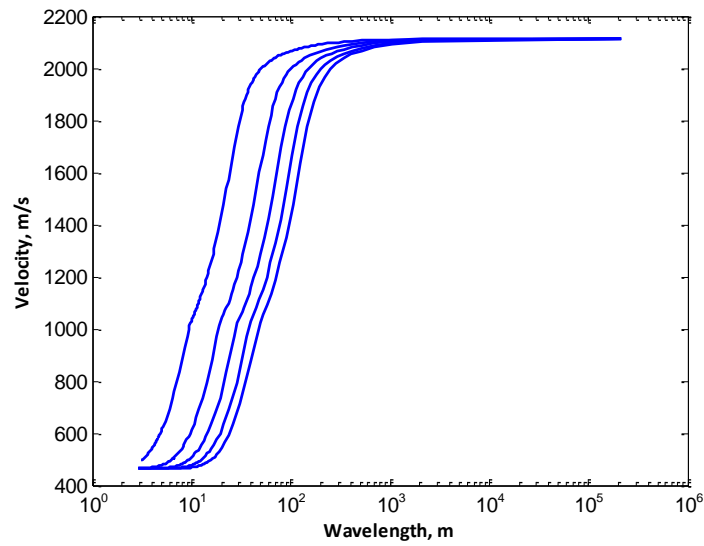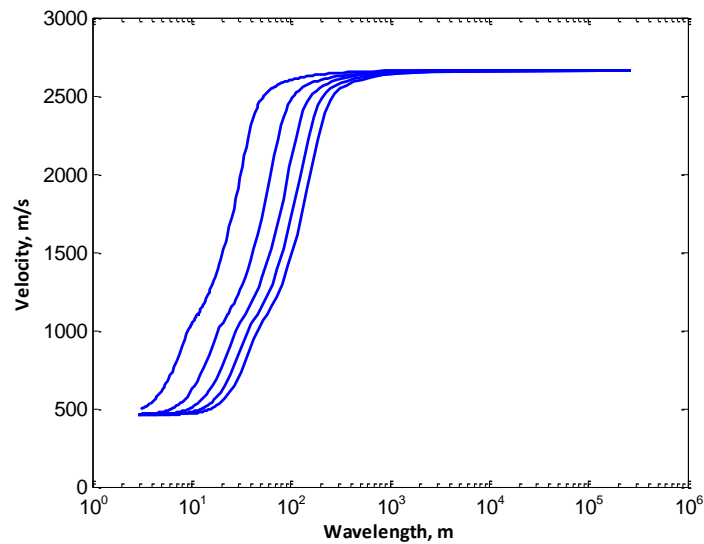
87
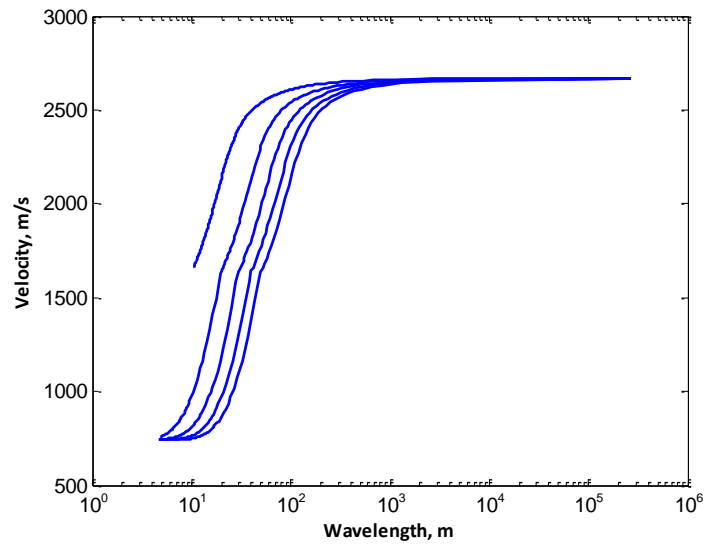
Figure A.9. A set of DCs obtained when the depth to bedrock changes from 2 m to 10 m in the increments of 2 m; the VSs of the layer and bedrock are held constant at 800 m/s and 2900 m/s, respectively.

88

# APPENDIX B: PICKING THE LOWER BEND FROM DISPERSION CURVE OF A

REAL-WORLD-DATASET
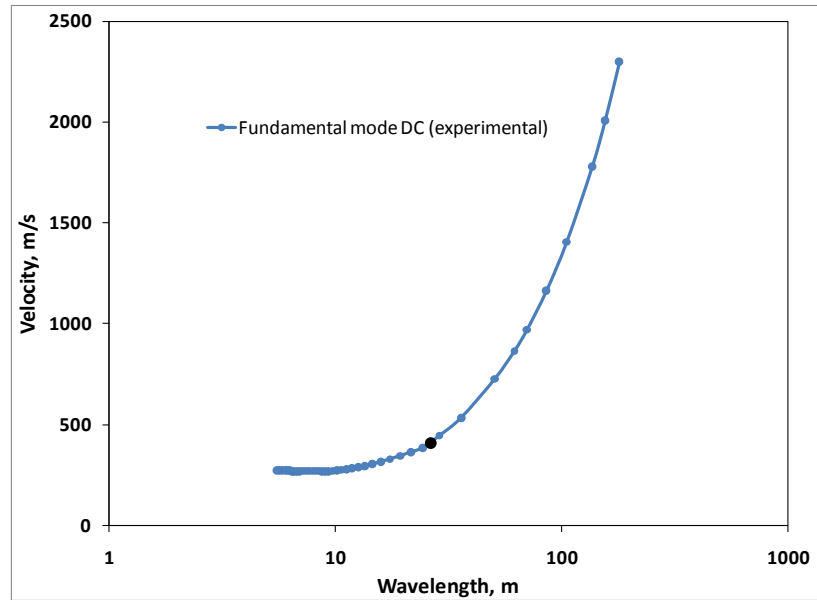
Figure B.1. Fundamental mode DC from Figure 5.2, plotted with respect to wavelength. The black dot in the curve shows the wavelength at which the lower bend is picked.

APPENDIX C: LIST OF ACRONYMS

AGC   Applied Geophysics Center

DC   Dispersion curve

HICB   High impedance contrast boundary

HVH   High-velocity halfspace

MASW   Multichannel Analysis of Surface Waves

RMS   Root-mean-square

SWAMI   Surface Wave Modal Inversion

VR   Rayleigh-wave velocity

VS   Shear-wave velocity

Vs30   Average VS of the upper 30 m

υ Poisson's ratio

REFERENCES

Beaty, K. S., Schmitt, D. R., & Sacchi, M. (2002). Simulated annealing inversion of multimode Rayleigh wave dispersion curves for geological structure. *Geophysical Journal International, 151*(2), 622-631.

Bergamo, P., Comina, C., Foti, S., & Maraschini, M. (2011). Seismic characterization of shallow bedrock sites with multi-modal Monte Carlo inversion of surface wave data. *Soil Dynamics and Earthquake Engineering, 31,* 530-534.

Calderón-Macías, C., & Luke, B. (2007). Improved parameterization to invert Rayleigh-wave data for shallow profiles containing stiff inclusions. *Geophysics, 72*(1), U1-U10.

Calderón-Macías, C., & Luke, B. (2010). Sensitivity studies of fundamental- and higher-mode Rayleigh-wave phase velocities in some specific near surface scenarios. In R. D. Miller, J. H. Bradford & K. Holliger (Eds.), *Advances in Near-Surface Seismology and Ground-Penetrating Radar* (Vol. 15, pp. 185-200). Society of Exploration Geophysicists, Tulsa: Geophysical Developments Series.

Casto, D., Calderón-Macías, C., Luke, B. & Kaufmann, R. (2010). Improving MASW results for a site with shallow bedrock through the use of higher-mode data. In D. Fratta, A. J. Puppala & B. Muhunthan (Eds.), *GeoFlorida 2010: Advances in Analysis, Modeling and Design,* Geotechnical Special Publication 199 (pp.1360-1368). Reston, Virginia: American Society of Civil Engineers.

Casto, D. W., Luke, B., Calderón-Macías, C., & Kaufmann, R. (2009). Interpreting surface-wave data for a site with shallow bedrock. *Journal of Environmental & Engineering Geophysics, 14(3),* 115-127.

Chik, Z., Islam, T., Mustafa, M. M., Sanusi, H., Rosyidi, S. A., & Taha, M. R. (2009). Surface wave analysis using Morlet wavelet in geotechnical investigations. *Journal of Applied Sciences, 9*(19), 3491-3501.

Foti, S., Sambuelli, L., Socco, V. L., & Strobbia, C. (2003). Experiments of joint acquisition of seismic refraction and surface wave data. *Near Surface Geophysics*, *1*, 119-129.

Gabriels, P., Snieder, R., & Nolet, G. (1987). In situ measurements of shear-wave velocity in sediments with higher-mode Rayleigh waves. *Geophysical Prospecting, 35*(2), 187-196.

Graff, K. F. (1975). *Wave motion in elastic solids.* New York, NY: Dover Publications.

Hebeler, G. L., & Rix, G. J. (2006). *Site characterization in Shelby County, Tennessee, using advance surface wave methods*. Report for Mid-America Earthquake Center, Georgia Institute of Technology, Atlanta, Georgia.

ICC (2006). *International Building Code*. International Code Council.

Jin, X., Luke, B., & Calderon-Macias, C. (2009). Role of forward model in surface-wave studies to delineate a buried high-velocity layer. *Journal of Environmental & Engineering Geophysics, 14*(1), 1-14.

Kansas Geological Survey (2006). *SurfSeis v2.0 MASW.* Kansas Geological Survey, Lawrence, Kansas.

Luke, B., & Calderón-Macías, C. (2007). Inversion of seismic surface wave data to resolve complex profiles. *Journal of Geotechnical and Geoenvironmental Engineering, 133*(2), 155-165.

Luke, B., Murvosh, H., Kittipongdaja, P., Karasa, A., Tamrakar, P., & Taylor, W. J. (2010). Rayleigh-wave dispersion curves for long, linear arrays at a predominantly-

gravel site. *Proceedings, Symposium on the Application of Geophysics to Engineering and Environmental Problems (SAGEEP), 23rd Annual Meeting* (pp. 742-750), Denver: Environmental and Engineering Geophysical Society.

Malagnini, L. (1996). Velocity and attenuation structure of very shallow soils: Evidence for a frequency-dependent Q. *Bulletin of the Seismological Society of America, 86*(5), 1471-1486.

Murvosh, H. (2011). *Complex VS Profiles to 100 m Depth from Rayleigh Waves and 3-D VS Model for Las Vegas Valley*. Master's thesis. University of Nevada Las Vegas, Nevada.

O'Neill, A., & Matsuoka, T. (2005). Dominant higher surface-wave modes and possible inversion pitfalls. *Journal of Environmental & Engineering Geophysics, 10*(2), 185-201.

Park, C. B., Miller, R. D., & Xia, J. (1999). Multichannel analysis of surface waves. *Geophysics, 64,* 800-808.

Park, C. B., Miller, R. D., Ryden, N., Xia, J., & Ivanov, J. (2005). Combined use of active and passive surface waves. *Journal of Engineering and Environmental Geophysics 10*(3), 323-334.

Pitilakis, K., Gazepis, C., & Anastasiadis, A. (2004). Design response spectra and soil classification for seismic code provisions. *Proceedings, 13th World Conference on Earthquake Engineering* (pp. 31-46). Vancouver, Canada: Canadian Association for Earthquake Engineering,

Rix, G. J., & Lai, C. G. (2005). *SWAMI v.1.2.0 – Surface Wave Modal Inversion Software*. Georgia Institute of Technology, Atlanta, Georgia.

Ryden, N. & Park, C. B. (2004). Fast simulated annealing inversion of surface waves on pavement using phase-velocity spectra. *Geophysics 71*(4), 49-58.

Sheriff, R. E. (2002). *Encyclopedic Dictionary of Exploration Geophysics*. Tulsa, Oklahoma: Society of Exploration Geophysicists.

Song, X., Gu, H., Liu, J., & Zhang, X. (2007). Estimation of shallow subsurface shear-wave velocity by inverting fundamental and higher-mode Rayleigh waves. *Soil Dynamics and Earthquake Engineering, 27*(7), 599-607.

Stokoe, K. H., Joh, S. H., & Woods, R. D. (2004). Some contributions of in situ geophysical measurements to solving geotechnical engineering problems. In A.V. Fonseca & P. W. Mayne (Eds.), *Proceedings, ISC-2 on Geotechnical and Geophysical Site Characterization* (pp. 97 - 132). Rotterdam: Millpress.

Strobbia, C., & Foti, S. (2006). Multi-offset phase analysis of surface wave data (MOPA). *Journal of Applied Geophysics, 59*(4), 300-313.

Supranata, Y. E. (2006). *Improving the Uniqueness of Shear-Wave Velocity Profiles Derived from the Inversion of Multiple-Mode Surface Wave Dispersion Data.* Ph.D. Dissertation, University of Kentucky, Lexington, KY.

Tamrakar, P. T., Luke, B., & Calderón-Macías, C. (2011). Practical considerations for characterizing shallowly buried bedrock using Rayleigh wave data, in N. Biggar, B. Luke & J. Werle (Eds.), *Proceedings, 43rd Annual Symposium on Engineering Geology and Geotechnical Engineering* (pp. 84-88)*. Pocatello, Idaho: Idaho State University.

Tokimatsu, K., Tamura, S., & Kojima, H. (1992). Effects of multiple modes on Rayleigh wave dispersion characteristics. *Journal of Geotechnical Engineering, 118*(10), 1529-1543.

Tselentis, G. A., & Delis, G. (1998). Rapid assessment of S-wave profiles from the
inversion of multichannel surface wave dispersion data. *Annali Di Geofisica, 41*(1),
1-15.

Werle, J.L. & Luke, B. (2007). Engineering with heavily cemented soils in Las Vegas,
Nevada. In A. J. Puppala, N. Hudyma, W. J. Likos (Eds.), *Proceedings, Problematic
Soils and Rocks and In Situ Characterization (pp. 162-171).* Reston, Virginia:
Geotechnical Special Publication.

Wood, C. M. (2009). *The Impact of Source Type, Source Offset, and Receiver Spacing on
Experimental MASW Data at Soft-Over-Stiff Sites.* Master's thesis, University of
Arkansas, Fayetteville, Arkansas.

Xia, J., Miller, R. D., & Park, C. B. (1999). Estimation of near-surface shear-wave
velocity by inversion of Rayleigh waves. *Geophysics, 64*(3), 691-700.

Xia, J., Miller, R. D., & Park, C. B. (2000). Advantages of calculating shear-wave
velocity from surface waves with higher modes: *70th Annual International Meeting,
,Expanded Abstracts,* Society of Exploration Geophysicists, Tulsa, Oklahoma, 1295–
1298.

VITA

Graduate College
University of Nevada, Las Vegas

Prajwol Tamrakar
Tibukchhen tole, Bhaktapur Municipality-8
Bhaktapur, Bagmati, Nepal

Degrees:
  Bachelor's degree in Civil Engineering, 2006
  Tribhuvan University, Nepal

Thesis Title: Effects of High-Impedance-Contrast Boundary upon Multi-modal Seismic
  Surface Wave Data

Publications:
Tamrakar, P. T., Luke, B., & Calderón-Macías, C. (2011). Practical considerations for
  characterizing shallowly buried bedrock using Rayleigh wave data, in N. Biggar, B.
  Luke & J. Werle (Eds.), *Proceedings, 43rd Annual Symposium on Engineering
  Geology and Geotechnical Engineering* (pp. 84-88). Pocatello, Idaho: Idaho State
  University.
Luke, B., Murvosh, H., Kittipongdaja, P., Karasa, A., **Tamrakar**, P., & Taylor, W. J.
  (2010). Rayleigh-wave dispersion curves for long, linear arrays at a predominantly-
  gravel site. *Proceedings, Symposium on the Application of Geophysics to Engineering
  and Environmental Problems (SAGEEP), 23rd Annual Meeting* (pp. 742-750),
  Denver: Environmental and Engineering Geophysical Society.

Thesis Examination Committee:
  Chairperson, Barbara Luke, Ph. D., P.E., P.G.E., F. ASCE
  Committee Member, Carlos Calderón-Macías, Ph.D.
  Committee Member, Douglas Rigby, Ph.D.
  Graduate Faculty Representative, Wanda Taylor, Ph. D.